Article

Cell Reports

Medulloblastoma Arises from the Persistence of a Rare and Transient Sox2^{+} Granule Neuron Precursor

Graphical Abstract

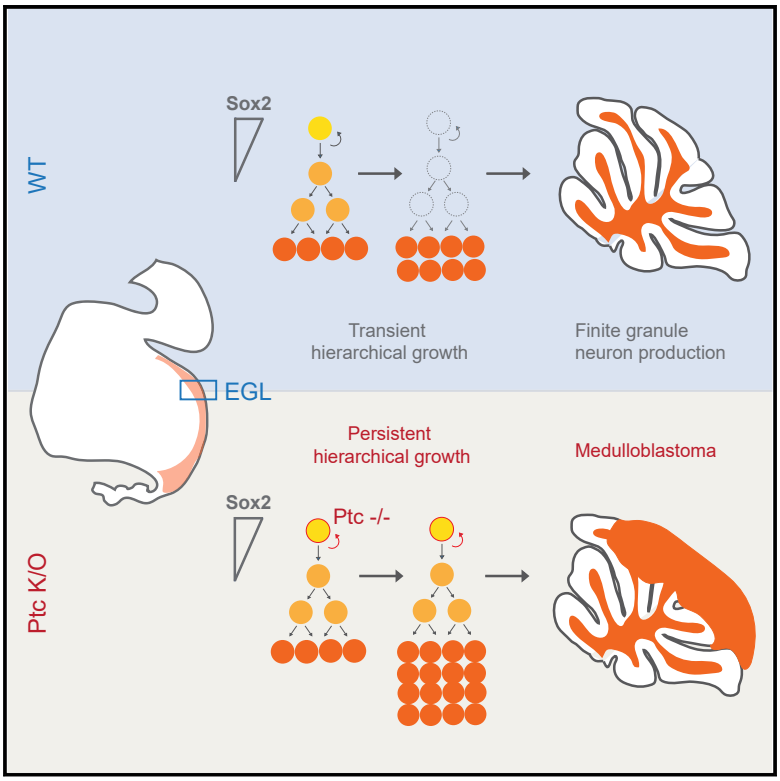

Authors

Hayden J. Selvadurai, Erika Luis, Kinjal Desai, ..., Arnold Kriegstein, Michael D. Taylor, Peter B. Dirks

Correspondence

peter.dirks@sickkids.ca

In Brief

Selvadurai et al. demonstrate that the developing cerebellar external germinal layer contains a transient population of more primitive cells expressing *Sox2*. Aberrant activation of the SHH signaling pathway in these cells causes persistent hierarchical growth, leading to medulloblastoma.

Highlights

- A rare and transient population of Sox2^{+} cells is identified in the developing EGL
- These stem-like Sox2^{+} cells contribute extensively to the granule lineage
- Constitutive activation of SHH in Sox2^{+} cells leads to their abnormal persistence
- Medulloblastoma arises from the sustained hierarchical output from these Sox2^{+} cells

Selvadurai et al., 2020, Cell Reports *31*, 107511
April 14, 2020
https://doi.org/10.1016/j.celrep.2020.03.075

CellPress

Cell Reports
Article

Medulloblastoma Arises from the Persistence of a Rare and Transient Sox2$^+$ Granule Neuron Precursor

Hayden J. Selvadurai,[1,2,11] Erika Luis,[1,2,3,11] Kinjal Desai,[1,2] Xiaoyang Lan,[1,2] Maria C. Vladoiu,[2,4] Owen Whitley,[3,5] Ciaran Galvin,[1,2] Robert J. Vanner,[1,2,3] Lilian Lee,[1,2] Heather Whetstone,[1,2] Michelle Kushida,[1,2] Tomasz Nowakowski,[6,7] Phedias Diamandis,[8,9] Cynthia Hawkins,[1,2,8,9] Gary Bader,[3,5] Arnold Kriegstein,[6,7] Michael D. Taylor,[1,2,4,10] and Peter B. Dirks[1,2,3,10,12,*]

[1]Developmental and Stem Cell Biology Program, The Hospital for Sick Children, Toronto, ON M5G 0A4, Canada
[2]Arthur and Sonia Labatt Brain Tumor Research Centre, The Hospital for Sick Children, Toronto, ON M5G 0A4, Canada
[3]Department of Molecular Genetics, University of Toronto, Toronto, ON M5S 1A8, Canada
[4]Department of Laboratory Medicine and Pathobiology, University of Toronto, Toronto, ON M5G 0A4, Canada
[5]The Donnelly Centre, University of Toronto, ON M5T 1W1, Canada
[6]Eli and Edythe Broad Center of Regeneration Medicine and Stem Cell Research, University of California, San Francisco, San Francisco, CA 94158, USA
[7]Department of Neurology, University of California, San Francisco, San Francisco, CA 94158, USA
[8]Department of Pathology, Toronto General Hospital, University Health Network, Toronto, ON M5G 2C4, Canada
[9]Division of Pathology, Hospital for Sick Children, Toronto, ON M5G 1X8, Canada
[10]Division of Neurosurgery, University of Toronto, Toronto, ON M5S 1A8, Canada
[11]These authors contributed equally
[12]Lead Contact
*Correspondence: peter.dirks@sickkids.ca
https://doi.org/10.1016/j.celrep.2020.03.075

SUMMARY

Medulloblastoma (MB) is a neoplasm linked to dysregulated cerebellar development. Previously, we demonstrated that the Sonic Hedgehog (SHH) subgroup grows hierarchically, with Sox2$^+$ cells at the apex of tumor progression and relapse. To test whether this mechanism is rooted in a normal developmental process, we studied the role of Sox2 in cerebellar development. We find that the external germinal layer (EGL) is derived from embryonic Sox2$^+$ precursors and that the EGL maintains a rare fraction of Sox2$^+$ cells during the first postnatal week. Through lineage tracing and single-cell analysis, we demonstrate that these Sox2$^+$ cells are within the Atoh1$^+$ lineage, contribute extensively to adult granule neurons, and resemble Sox2$^+$ tumor cells. Critically, constitutive activation of the SHH pathway leads to their aberrant persistence in the EGL and rapid tumor onset. We propose that failure to eliminate this rare but potent developmental population is the tumor initiation mechanism in SHH-subgroup MB.

INTRODUCTION

Medulloblastoma (MB) is the most common malignant brain tumor in children (Dolecek et al., 2012) and intrinsically linked to aberrant cerebellar development. Tumors are a functionally heterogeneous mix of cells, with only a fraction of neural stem-like cells able to propagate the disease in transplantation assays (Read et al., 2009; Singh et al., 2004; Ward et al., 2009). We have previously demonstrated through genetic lineage tracing that *in situ* growth of Sonic Hedgehog (SHH)-subtype MB is driven hierarchically, with rare and quiescent cells expressing the transcription factor (TF) Sox2 generating the tumor mass. Downstream progeny consist of rapidly proliferating Doublecortin (DCX) expressing progenitors and Neuronal nuclear antigen (NeuN) expressing differentiated cells with limited survival (Vanner et al., 2014). This neoplastic stem cell-driven hierarchy is highly reminiscent of a normal neurogenic process.

The diverse cell types that make up the mature cerebellum originate from two distinct germinal centers during embryonic cerebellum development: the ventricular zone (VZ) and the rhombic lip (RL). The VZ is a layer of cells lining the ventral surface of the cerebellar anlage that give rise to all γ-aminobutyric acid (GABA)-ergic neurons and glial cell lineages. Cell fate is specified from the VZ beginning around embryonic day (E) 10.5 in mouse and continues until the third postnatal week from progenitors that delaminate from the VZ and divide in the nascent white matter (WM) (Sudarov et al., 2011). The RL is a transient zone in the most rostral aspect of the cerebellar anlage forming the interface between the VZ and roof plate ectoderm (Wingate, 2001). Signaling molecules such as TGF-β derived from the roof plate specify glutamatergic cell fate in RL cells (Hatten, 1999). Deep cerebellar nuclei neurons are the first to be specified from E10.5, followed by the major RL output: granule neuron progenitors (GNPs). These are born at the RL ~E12.5–E16.5 and migrate rostrally across the pial surface of the cerebellum to form a transient secondary germinal zone, the external germinal layer (EGL). During this phase GNPs undergo multiple rounds of transit amplification driven by the SHH mitogen (Wallace, 1999;

Wechsler-Reya and Scott, 1999), before exiting the cell cycle and migrating radially away from the pial surface as they differentiate into mature granule neurons (GNs) within the internal granular cell layer (IGL) by postnatal day (P) 21 in the mouse and after the first year in human.

Given the role of SHH in driving GNP proliferation, it is unsurprising that about one-third of MBs are characterized by elevated levels of SHH pathway activity (Northcott et al., 2012). Disruption of normal GN development through activating mutations in SHH pathway components is therefore widely accepted as an initiating event in SHH-subtype MB. In support of this, mouse models of the disease with germline mutations activating the pathway have revealed a characteristic process of EGL hyperplasia (Goodrich et al., 1997; Oliver et al., 2005) and subsequent MB onset after the acquisition of further oncogenic mutation, such as those targeted to *Tp53* or *Cdkn2a* (Tamayo-Orrego et al., 2016). Targeting constitutive SHH pathway drivers to the embryonic neural stem cell (NSC) fraction (defined by GFAP or Olig2 expression) also leads to MB, though only after specification to the granule lineage (Schüller et al., 2008; Yang et al., 2008). Combined with evidence for a cellular hierarchy in MB (Read et al., 2009; Vanner et al., 2014; Ward et al., 2009), these data present a compelling picture of SHH-subtype MB arising and progressing through aberrantly sustained GN development. Although our previous data suggests that $Sox2^+$ tumor cells may drive this cellular process in MB, the extent to which $Sox2^+$ cells might determine the normal development of the granule lineage and contribute to MB initiation is not clear.

Sox2 codes for a high-motility group TF now well established as a core regulator of stem cell function in development, adult tissue homeostasis, and cancer through wide-ranging and context-dependent epigenetic mechanisms (Arnold et al., 2011). In the brain, Sox2 is expressed in radial glia during early development and in NSCs in the adult (Ellis et al., 2004). Functional approaches have revealed an essential requirement for Sox2 in cortical neurogenesis (Favaro et al., 2009) but this has not been explored to the same extent in the developing cerebellum. Recent data also support an important role for Sox2 in maintaining stem cell state in both mouse and human forebrain glioma (Favaro et al., 2014; Gangemi et al., 2009). In human MB, SOX2 expression has been shown to be associated with the SHH subtype (Ahlfeld et al., 2013), with higher bulk expression levels correlating with a poorer prognosis (Vanner et al., 2014).

In this study, we tested the hypothesis that normal GN development is rooted in a $Sox2^+$ cell-driven hierarchy. We demonstrate that expression of Sox2 persists in a small fraction of cells in the early developing EGL that retain a more primitive state. These cells contribute extensively to granule lineage development and maintain this cellular process in the context of constitutive SHH activation, leading to MB formation. These findings reinforce the parallels between normal development and cancer and offer insight into the temporal window of vulnerability for oncogenic transformation of the developing cerebellum. We propose a model of how cancers initiate under the influence of SHH activation, through the persistence of a rare developmental population that seeds hierarchical growth from the earliest stages of neoplasia.

RESULTS

Abundant Sox2 Expression Becomes Restricted to the VZ and RL Germinal Centers during Embryonic Cerebellum Development

In order to test the hypothesis that the $Sox2^+$ cells maintaining SHH-active neoplastic growth are derived from an analogous cell during development, we first analyzed the expression of Sox2 in the embryonic mouse cerebellum with a *Sox2-eGFP* reporter mouse line (Ellis et al., 2004). We detected widespread reporter activity (GFP^+ cells) in the cerebellum at E10.5 (Figures S1A and S1B) and E12.5 (Figures 1A and S1C), which very closely matched the native Sox2 protein detected by immunofluorescence (IF). Sox2 expression at E12.5 was also abundant at the emergent RL, as defined by expression of Pax6 (Figure 1B), a downstream effector of the pro-glutamatergic TF Atoh1 (Mansouri et al., 1994; Schedl et al., 1996; Yeung et al., 2014). By E14.5, Sox2 expression was largely restricted to the VZ and RL (Figures 1C, 1D, and S1D), germinal centers for GABAergic and glutamatergic neuronal lineages, respectively.

Lineage Tracing Shows that the EGL Is Derived from a Population of $Sox2^+$ Precursors

To determine the output of $Sox2^+$ RL cells, we performed a series of Sox2 lineage-tracing experiments from time points corresponding to the initiation and expansion of the GN lineage. We used mice harboring the $Sox2^{CreERT2}$ inducible cre-recombinase allele (Arnold et al., 2011) in combination with a *Rosa26 CAG-loxP-stop-loxP-tdTomato* ($R26^{tdT}$) red fluorescent reporter allele (Madisen et al., 2010) to indelibly mark any cell expressing Sox2 and its progeny upon tamoxifen (TMX) administration. Marking $Sox2^+$ cells at E10.5 led to reporter activation in virtually all cerebellar cells (Figure S1E). Tracing from E12.5 caused reporter expression in the majority of cells at the RL and nascent EGL after 24 or 48 h (Figures 1E, 1F, and S1F), suggesting that the newly specified EGL is derived from a $Sox2^+$ population present within the E12.5 VZ/RL. We next initiated a lineage trace at E14.5 to determine if the $Sox2^+$ population identified within the RL at this time point continues to contribute to the expanding GN lineage. This experiment revealed more restricted activation of the reporter in both the RL and the EGL (Figures 1G and S1G), with the majority of labeled EGL cells residing in the outer layer (Figure 1G). Littermates lacking Cre or cohorts without TMX administration were used as negative controls, and no tdT expression was observed in these cases. These lineage-tracing experiments suggest that the EGL is derived from a population of $Sox2^+$ progenitors in the VZ/RL germinal centers and that $Sox2^+$ cells are maintained as a sub-population of the RL and early EGL, contributing to early GNP development.

Heterogeneous Expression of Sox2 in the Embryonic EGL and Persistence in the Postnatal EGL

We next examined the expression of Sox2 within the RL. At E14.5, Sox2 expression was higher in the cells of the inner RL (iRL), directly adjacent to the VZ (Figure 2A). However, expression of Sox2 was also evident in the external RL (eRL) and nascent

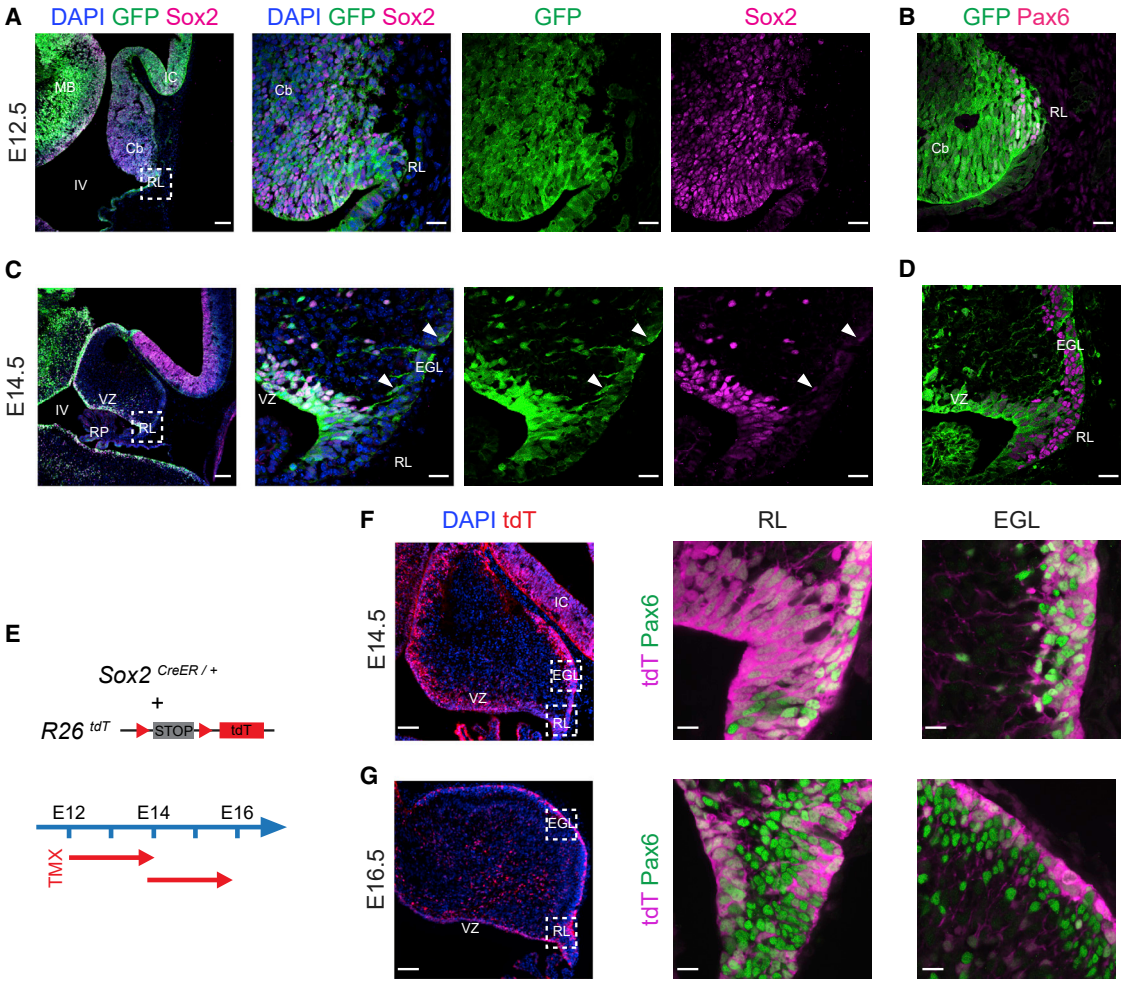

Figure 1. The EGL Is Derived from Sox2^{+} Progenitors in the Embryonic RL

(A) Expression of *Sox2-eGFP* transgene fluorescence and endogenous Sox2 protein detected by IF in the medial cerebellum at E12.5. Scale bars, 100 μm (left panel) and 20 μm (remaining panels). Cb, cerebellum; IC, inferior colliculus; IV, fourth ventricle; MB, midbrain; RL, rhombic lip.

(B) Pax6 expression marks the cellular output of the RL at E12.5. Scale bar, 20 μm.

(C and D) By E14.5, Sox2 expression becomes restricted to the VZ and RL (C), with cells exiting the RL, marked by Pax6 (D), showing heterogeneous Sox2 expression (arrowheads mark Sox2^{+} cells). EGL, external germinal layer; RP, roof plate. Scale bars as in (A) and (B).

(E) Lineage-tracing strategy following TMX induction at E12.5 or E14.5 to Sox2^{CreER} ; R26^{tdT} embryos.

(F) Analysis of tdT reporter expression and its co-localization with Pax6 at E14.5 following E12.5 induction at VZ and RL germinal regions. Scale bars, 100 μm (left panel) and 12 μm (remaining panels).

(G) Analysis of tdT reporter expression and its co-localization with Pax6 in the cerebellum at E16.5 following E14.5 induction. Scale bars as in (F).

posterior EGL (pEGL), suggesting the possible maintenance of expression in a subset of cells transitioning to a glutamatergic identity. In contrast, Pax6 expression showed high levels within the eRL and pEGL alongside relatively lower levels in cells within the iRL and adjacent VZ (Figure 2B). The regionalization of the RL defined by Sox2 expression is consistent with previous findings (Yeung et al., 2014) and is suggestive of most cells transitioning from a Sox2-high/Pax6-low state to a Sox2-low/Pax6-high state upon acquisition of granule lineage identity.

Sox2 also showed heterogeneous expression within the E14.5 EGL (Figure 2C), consistent with our observation that a Sox2 lineage trace from E14.5 results in the marking of cells within the EGL. Analysis of the EGL at E16.5, by which point GNP migration has progressed to the most rostral aspect of the cerebellum, revealed heterogeneous expression of Sox2 similar to that observed at E14.5 (Figures 2D, S2B, and S2C). Analysis of the EGL at birth (P0) revealed a small fraction of cells maintaining Sox2 expression (Figures 2E and S2D). Sox2^{+} cells were detected both at the outer EGL and within the inner EGL adjacent to the molecular layer. Sox2/GFP expression was also detected in the developing glial and interneuron lineages derived from the VZ/WM, as expected. By P7, near the peak of GNP proliferation, Sox2 expression was extremely rare within the EGL (Figure S2E), detectable only in a few cells per cerebellum section. These results support a potential role for Sox2 in the protracted expansion of the granule lineage for the first postnatal week.

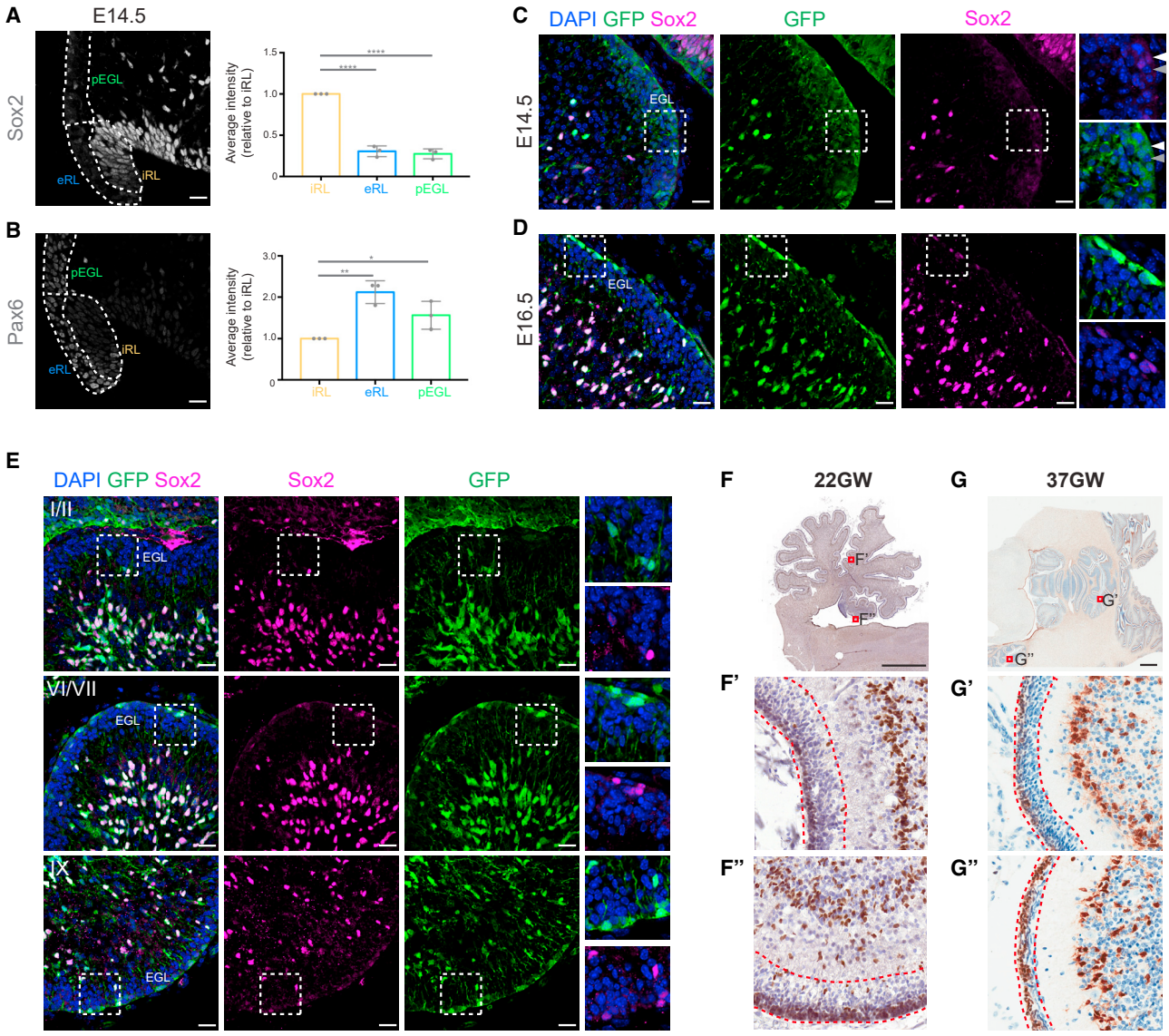

Figure 2. Expression of Sox2 Is Maintained in the Nascent EGL and Persists until Birth in Mouse and Human

(A) Expression of endogenous Sox2 protein detected by IF in the external RL (eRL), inner RL (iRL), and posterior EGL (pEGL) at E14.5 and quantification of the average per-cell intensity (relative to iRL). Scale bar, 20 μm; n = 3; error bars denote mean ± SEM; *p < 0.05, **p < 0.01, and ***p < 0.0001 (two-tailed unpaired t test).

(B) Expression of endogenous Pax6 protein detected by IF in the eRL, iRL, and pEGL at E14.5 and quantification of the average intensity (relative to iRL). n = 3; error bars denote mean ± SEM; two-tailed unpaired t test. Scale bar as in (A).

(C) Overlapping heterogeneous expression of *Sox2-eGFP* transgene and endogenous protein in the EGL at E14.5. Magnified area shows $Sox2^{+}$ cells (white arrowhead) alongside $Sox2^{-}$ cells (gray arrowhead). Scale bars, 20 μm.

(D) Sox2 expression in the EGL at E16.5. $Sox2^{+}$ cells are marked by white arrowheads in magnified area. Scale bars as in (C).

(E) Expression of *Sox2-eGFP* reporter and endogenous Sox2 protein detected by IF. Representative images showing the EGL of nascent lobules I/II, VI/VII, and XI are shown, with magnified regions showing the overlap between GFP and endogenous Sox2 expression within the EGL. Scale bars, 20 μm.

(F and G) Primary human cerebellum from GW22 (F) and GW37 (G) stained for Sox2 by IHC. EGL demarcated in red (F′, F″, G′, and G″). Scale bar, 2 mm for both.

Identification of Sox2 Expression in Developing Human EGL

The cerebellum develops across mammalian species following the same cellular mechanisms and core lobe patterning as those described in the mouse, with an increase in foliation complexity and a much more protracted period of granule neurogenesis in humans. The EGL is first detected around the 10th gestational week (GW) and persists up to the second year of life (Rakic and Sidman, 1970). Proliferation within the EGL peaks between GW28 and GW34, equivalent to the early postnatal stage in mouse (Abrahám et al., 2001). To test if our mouse observations translate to the human

context, we assessed Sox2 expression in the developing human cerebellum. We performed immunohistochemistry (IHC) for Sox2 on GW22- and GW37-stage primary human cerebellum tissue and found a high degree of foliation and clear lamination within each nascent lobule (Figures 2F and 2G). Expression of Sox2 was strikingly abundant within the EGL, with a particular density in the outer EGL. Consistent with our observation in mouse, we noted that the frequency of $Sox2^+$ cells within the EGL was spatially heterogeneous and not equal across all folia.

$Sox2^+$ Cells in the P0 EGL Display Characteristics of a Progenitor Cell State

To shed further light on the cellular identity of $Sox2^+$ cells identified in the mouse P0 EGL, we analyzed Sox2 expression alongside the intermediate progenitor marker DCX and the neuronal marker NeuN. Expression of these markers is indicative of GNP exit from the cell cycle and commitment to a terminally differentiated GN identity. Expression of both DCX and NeuN was mutually exclusive with Sox2 in the EGL, except for a rare occurrence when we noted GFP expression co-localizing with low levels of DCX (Figures 3A and 3B). We further assessed expression of Pax6 alongside Sox2 as a marker of granule lineage identity and found overlapping expression in the majority of $Sox2^+$ cells (Figures 3C and S3A).

We analyzed the expression of GFP alongside putative NSC markers Nestin and Olig2, which have both been shown to mark rare fractions of cells in the developing EGL (Li et al., 2013; Wojcinski et al., 2017, 2019). Although some overlap was evident, we could not conclusively determine whether all Sox2 expressing cells we identified also expressed Nestin, because of the filamentous nature of its cytoplasmic staining (Figure S3B). Olig2 expression was not present within the EGL but did co-localize with Sox2 expression in scattered cells within the developing IGL (Figure S3C).

To examine the $Sox2^+$ EGL cells at a functional level, we next probed their cell cycle dynamics through an EdU pulse experiment. EdU incorporation was widespread through the EGL (Figure 3D), indicative of abundant proliferation. However, EdU incorporation within the $Sox2^+$ EGL fraction occurred at significantly lower levels (11.87% ± 3.53%) compared with the $Sox2^-$ fraction (25.34% ± 1.19%) (Figure 3E), suggesting that $Sox2^+$ cells are functionally distinct from the surrounding progenitors. Combined, these data suggest that the majority of $Sox2^+$ EGL cells are committed to the granule lineage and may exist in a more primitive state than surrounding GNPs.

$Sox2^+$ EGL Cells Are Derived from the *Atoh1*$^+$ Lineage

EGL cells displaying hallmarks of a more primitive state have been described previously, though they appear to be derived from the VZ (Li et al., 2013; Wojcinski et al., 2017). To investigate the source of the $Sox2^+$ EGL population, we performed a set of lineage-trace experiments using mice with the constitutively active *Atoh1*^{Cre} recombinase allele (Matei et al., 2005) crossed to the *R26*^{tdT} reporter mouse line (Figure 3F). *Atoh1* expression defines the RL-derived glutamatergic lineages from ~E10.5 (Akazawa et al., 1995; Ben-Arie et al., 1996, 1997). This model caused labeling of all *Atoh1*-derived progeny, including clear labeling of the EGL as expected in the P0 cerebellum (Figure 3G). To validate the model, we traced mice to adulthood and found the entire granule lineage marked by the reporter (Figures S3D and S3E), with the exception of lobe X, which shows a distinct lack of labeling at both P0 and in adulthood.

Within the EGL of *Atoh1* traced mice, we identified $Sox2^+$ cells marked by the tdT label, confirming their identity as cells within the granule lineage (Figure 3H). However, we also observed $Sox2^+$ cells within the EGL that lacked the tdT label. Although we cannot exclude the possibility of some cells' not recombining the reporter despite *Atoh1* expression, given the extensive reporter labeling through the rest of the EGL and subsequent GNs, we do not think this would apply in every case, raising the possibility that the EGL could contain more primitive cells from both RL and VZ origins. To examine this, we crossed the *Atoh1*^{Cre}*; R26*^{tdT} line to mice harboring the *Sox2*^{eGFP} transgene to perform flow cytometry analysis on the basis of both tdT (RL-derived) and GFP ($Sox2^+$) expression (Figures 3I, 3J, S3F, and S3G). After first gating on tdT expression, we detected the presence of a small fraction of tdT/GFP double-positive cells (3.24% ± 0.61%). Combined, these data support the hypothesis that a fraction of cells derived from the *Atoh1*$^+$ lineage maintain expression of Sox2 during EGL development.

ScRNA-Seq Analysis of P0 Mouse Cerebellum Supports the Presence of a More Primitive $Sox2^+$ GNP Cell State Reminiscent of $Sox2^+$ MB Cells

To further interrogate the characteristics of $Sox2^+$ precursors within the Atoh1 lineage, we independently examined single-cell RNA sequencing (scRNA-seq) data of the developing mouse cerebellum (Vladoiu et al., 2019). Unsupervised clustering using Uniform Manifold Approximation and Projection (UMAP) (McInnes et al., 2018) was performed on the individual cell transcriptomes of 4,409 cells collected at P0. Cell-cycle signatures were regressed to reduce confounding sources of variation, and 13 unique clusters were identified (Figures 4A, S4A, and S4B). Cluster identities were assigned using expression of established markers as well as the cell identities resolved previously across multiple embryonic and postnatal time points, with granule lineage cells being the most abundant cell type (Figure 4B).

The GNP compartment encompassed clusters 2 and 4, which were strongly enriched in the expression of RL lineage marker Atoh1 and had negligible expression of the VZ lineage marker Ptf1a (Figure 4C). They also scored the most strongly for S and G2/M proliferation signatures (Tirosh et al., 2016; Figures 4D and S4G). The identification of two discrete GNP clusters is consistent with the original description of these data (Vladoiu et al., 2019). To interrogate heterogeneity in the GNP compartment, we extracted the 1,104 GNPs from clusters 2 and 4 and performed additional unsupervised clustering following cell-cycle regression, revealing four unique sub-clusters (Figures 4E–4G, S4C, and S4D), including one (sub-cluster 3, 3.89%) that was positive for both granule lineage (Atoh1, Pax6) and NSC (Sox2, Gfap) markers but relatively deficient in proliferation markers (Mki67, Top2a) (Figures 4F and S4E). Assessment of differential gene expression confirmed the identity of sub-cluster 3

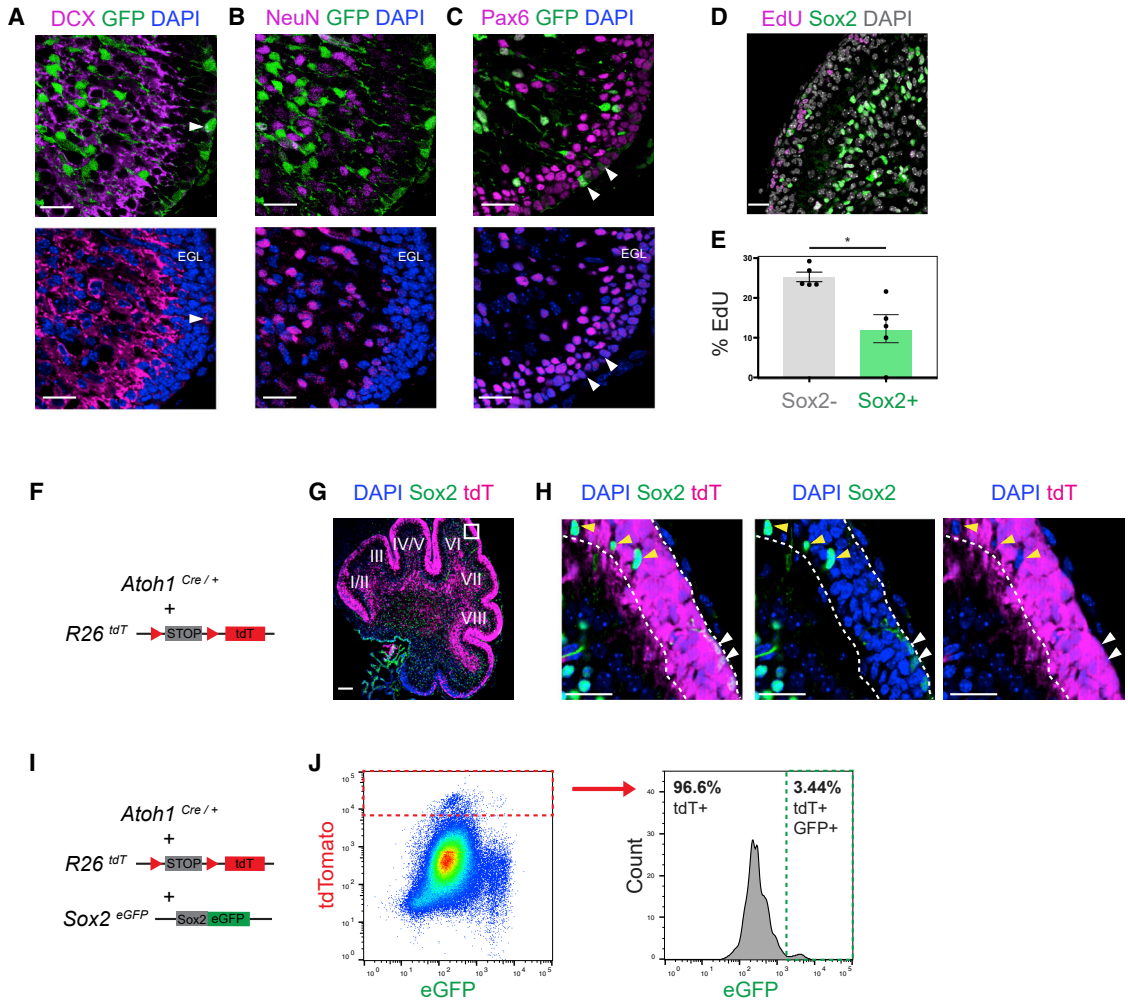

Figure 3. Sox2^{+} Overlaps with Markers of GNPs in the Postnatal EGL

(A and B) Rare overlapping GFP and DCX expression was observed in the P0 EGL (A, arrowhead), while no overlap was seen between GFP and NeuN (B). Scale bars, 20 μm.

(C) All GFP^{+} external EGL cells were Pax6^{+} (arrowheads). Scale bars, 20 μm.

(D) Representative IF images of endogenous Sox2 protein and EdU at 3 h post-injection. Scale bar, 20 μm.

(E) Quantification of EdU incorporation (in D) in Sox2^{+} and Sox2^{-} cells ($p = 0.0166$). n = 5; error bars denote mean ± SEM; two-tailed paired t test.

(F) Lineage-tracing strategy in Atoh1^{Cre} ; R26^{tdT} mice.

(G) Representative IF images of endogenous Sox2 protein and tdT reporter expression in the P0 cerebellum. Scale bar, 100 μm.

(H) Magnified image from (G) illustrating heterogeneous Sox2 expression with clear Atoh1 lineage^{+} (white arrowheads) and Atoh1 lineage^{-} (yellow arrowheads) origins. Scale bars, 20 μm.

(I) Atoh1^{cre} ; R26^{tdT} ; Sox2^{eGFP} transgenic mice were bred for fluorescence-activated cell sorting (FACS) analysis of Sox2^{+} cell lineage origins.

(J) Representative FACS plot indicating typical population distribution of tdT and GFP expression from the P0 hindbrain (left). Histogram of tdT^{+} cells showing percentage of Sox2^{+} cells derived from the Atoh1 lineage (right).

as an Atoh1^{high} Sox2^{high} compartment of GNPs (Table S1), with all genes (except Pax6) being statistically differentially expressed ($p < 0.001$). To interrogate the functional properties of these cells, we applied S and G2/M signature enrichment scoring and found that the Atoh1^{high} Sox2^{high} cluster exhibited a significant reduction in S and G2/M scores. Furthermore, Atoh1^{high} Sox2^{high} cells displayed a reduced similarity to P0 GNs (P0 cluster 0) and increased similarity to P0 glial cells (P0 cluster 1) (Figure 4H). Pathway analysis (Figure 4I; Table S2) in sub-cluster 3 using g:Profiler (Reimand et al., 2016) revealed differential enrichment in pathways reflective of the reduced proliferation in Atoh1^{high} Sox2^{high} cells (upregulation of translation and ribosome biogenesis, downregulation of cell cycle). Interestingly, several neurogenic pathways were also enriched in this sub-cluster, including nervous system development and regulation of neuron differentiation. Of note, we also compared the Atoh1^{high} Sox2^{high} cluster with the remaining GNPs for SHH pathway enrichment and found no measurable difference, suggesting that Atoh1^{high} Sox2^{high} cells are similarly SHH active to their more differentiated GNP counterparts (Figure S4I). We

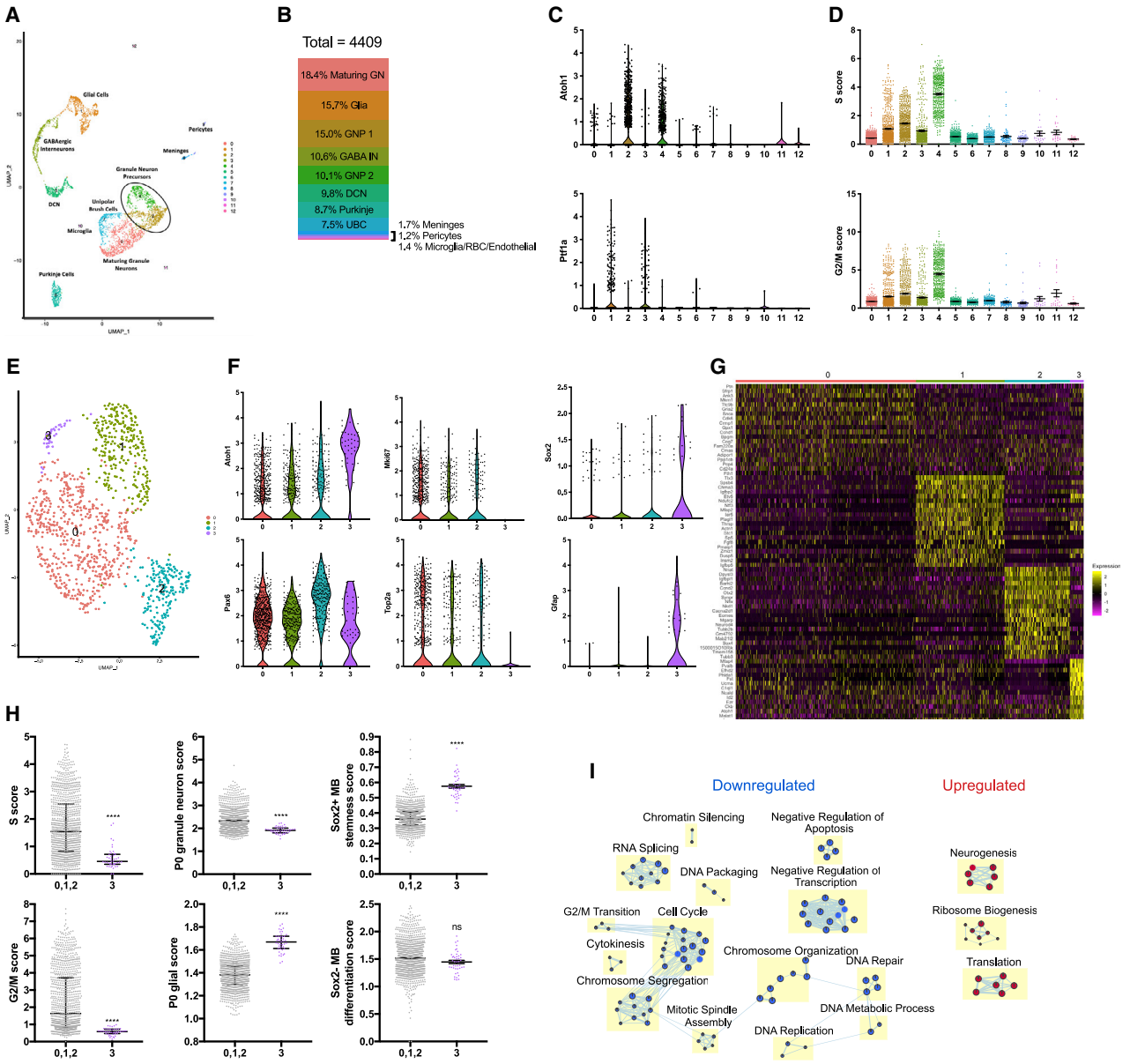

Figure 4. scRNA-Seq Reveals a Distinct Cluster of Atoh1^{high} Sox2^{high} GNPs

(A) Uniform Manifold Approximation and Projection (UMAP) visualization of transcriptionally distinct cell populations from 4,409 cells from the P0 mouse cerebellum.

(B) Relative composition of different clusters at P0 from (A).

(C) Violin plots indicating expression of Atoh1 and Ptf1a across clusters.

(D) Scatterplot by P0 clusters illustrating individual cells' scores for enrichment of S (top) and G2/M (bottom) signatures (mean ± SEM).

(E) UMAP visualization of transcriptionally distinct sub-clusters following re-clustering of the 1,104 GNPs.

(F) Violin plots indicating expression of Atoh1, Pax6, Mki67, Top2a, Sox2, and Gfap across GNP sub-clusters.

(G) Heatmap indicating expression of the 20 most significant genes identifying each GNP sub-cluster signature. Genes upregulated in yellow, downregulated in purple.

(H) Scatterplots of GNP sub-cluster 3 versus all other GNPs (cluster 0, 1, and 2) illustrating individual cells' scores for enrichment of S, G2/M, P0 GN, P0 glial, Sox2^{+} MB stemness, and Sox2^{-} MB differentiation signatures. ****$p < 0.0001$; ns, not significant. Mean ± SEM; two-tailed Mann-Whitney test.

(I) Enrichment map of Gene Ontology (GO) biological pathway terms upregulated (red) and downregulated (blue) in Atoh1^{high} Sox2^{high} (GNP sub-cluster 3) cells.

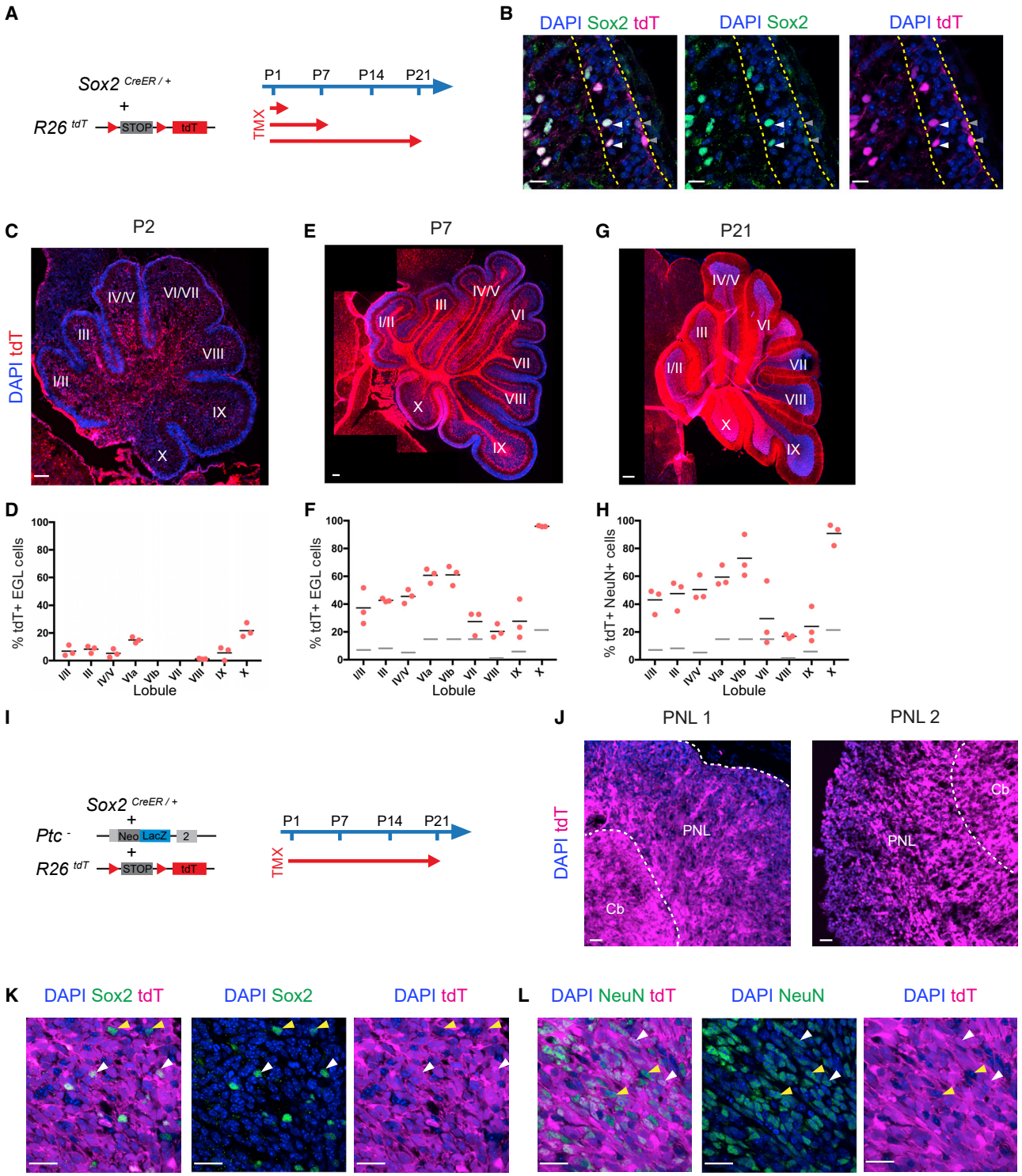

Figure 5. Sox2^{+} GNPs Contribute Extensively to the Granule Lineage and to Lesions in Ptc$^{+/-}$ Germline Mutants

(A) Strategy for TMX induction in Sox2^{CreER} ; R26^{tdT} pups at P1 followed by analysis of reporter expression.

(B) Rare tdT labeling within the EGL (outlined area) at P2 consistent with expression of endogenous Sox2 protein detected by IF (white arrowheads, relatively high Sox2 expression; gray arrowheads, relatively low Sox2 expression). Scale bars, 12 μm.

(C and D) Representative IF image of tdT reporter expression in the P2 cerebellum (C) and quantification of the percent tdT^{+} cells in the EGL (D). Bar denotes mean; n = 3 biological replicates from at least two litters for each data point. Scale bar, 100 μm.

(legend continued on next page)

next examined whether cells with a similar signature are present at P7 (Vladoiu et al., 2019). P7 GNPs expressing the Atoh1^{high} Sox2^{high} P0 GNP signature were not identified, confirming the temporal restriction of the Atoh1^{high} Sox2^{high} pool (Figure S4J). Combined, these data are consistent with a model in which rare, primitive Atoh1^{high} Sox2^{high} cells lie at the root of hierarchical expansion before commitment to a differentiated cell fate and concomitant expression of more mature markers such as Neurod1, Stmn1, Fabp7, and Tubb5.

We next compared these GNP clusters to the Sox2^{+} and Sox2^{-} fractions we characterized previously in SHH-subtype MB (Vanner et al., 2014). Supporting the link between granule lineage development and MB, the Atoh1^{high} Sox2^{high} GNPs displayed significant enrichment for the primitive Sox2^{+} MB gene expression signature, while no group of P0 GNPs were enriched for the more differentiated Sox2^{-} fraction of MB (Figure 4H). As a control, we scored all P0 cell types for the same stem and differentiated signatures (Figure S4H) and found that P0 glial cells bore highest similarity to Sox2^{+} MB cells. In contrast, maturing GNs exhibited greatest similarity to Sox2^{-} MB cells, indicating that the MB tumor bulk is more similar to terminally differentiated GNs than progenitors of the EGL. Combined, these observations strongly support a similar model of Sox2-driven hierarchical growth in both granule lineage development and MB.

Lineage Tracing from Sox2^{+} GNPs in Newborn Mice Reveals Extensive Contribution to the Granule Lineage and MB

To determine the extent to which Sox2^{+} EGL cells contribute to expansion of the GNP population, we performed a set of Sox2 lineage-tracing experiments in newborn pups using the *Sox2^{CreERT2}* recombinase and *R26^{tdT}* reporter alleles (Figure 5A). After inducing at P1 and tracing for 24 h, tdT expression was analyzed alongside IF for Sox2, which revealed a labeling pattern largely consistent with endogenous Sox2 expression (Figure 5B), though with rare exceptions (Figure S5A). Reporter activation was widespread within the WM and IGL, consistent with the broad expression of Sox2 in VZ-derived cells (Figures 5C and S5B). Analysis of the EGL at each nascent lobule revealed a reproducible, spatially specific pattern of reporter activation, indicative of regional differences in Sox2 expression at this time point (Figure S5B). In each quantified region, except for lobule X, the proportion of acutely labeled cells was less than 10% of total EGL cells (Figure 5D).

We then tested the contribution of this rare labeled cell fraction to GNP production in the EGL by analyzing tdT reporter expression at P7, 6 days after TMX induction, and found it to be abundant within the EGL (Figures 5E and S5C), consistent with extensive cellular expansion from the initially labeled Sox2^{+} cell fraction. Quantification of tdT^{+} EGL cells revealed on average at least a 3-fold increase in the proportion of labeled cells (Figure 5F), demonstrating that the contribution of Sox2^{+} cells to subsequent GNPs is greater than the Sox2^{-} cell fraction (otherwise we would expect a balanced output with the labeled cell fraction remaining the same). Analysis of the IGL after tracing from P1 to P21 revealed a pattern of lobule-specific reporter expression, with differences between groups I–VI, VII–IX, and X (Figures 5G and S5D). In order to quantify the proportion of tdT labeled GNs, we co-stained for NeuN, allowing GNs to be distinguished from other Sox2-derived cell types within the IGL (Figure S5E). The fraction of tdT labeled GNs at P21 showed a striking concordance with the fraction of labeled EGL cells from matched regions quantified at P7 (Figure 5H), consistent with a balanced expansion of all remaining GNPs after loss of Sox2^{+} cells in the first week of postnatal growth. Combined, these data reveal the persistence of a potent Sox2^{+} progenitor population within the EGL that is maintained into the first week of postnatal life with an enhanced capacity for neurogenesis.

We next tested the hypothesis that these Sox2^{+} GNPs could act as the root of neoplastic growth in the context of a germline *Ptc1* heterozygous mouse model. We have previously shown that MB grows hierarchically, with a fraction of Sox2^{+} cells generating more rapidly cycling DCX^{+} progeny, which undergo terminal differentiation into post-mitotic NeuN^{+} cells. Using mice harboring the widely used *Ptc^{LacZ}* germline null allele (*Ptc^{-}*) (Goodrich et al., 1997), we performed the same lineage trace from P1 as above to test whether hierarchical neoplastic growth is present from the earliest stages of tumor development (Figure 5I). Indeed, assessment of pre-neoplastic lesions (PNLs) at P21 revealed extensive labeling of the majority of tumor cells (Figure 5J), including cells expressing Sox2 (Figure 5K) and NeuN (Figure 5L). Although not every cell expressed the tdT label, we suggest that this is likely due to initiation of tumorigenic growth prior to tdT induction. These data provide strong evidence for neoplastic growth rooted in the potential transformation of cells in the Sox2^{+} GNP fraction and perpetuated by population-level self-renewal of Sox2^{+} cells during disease progression.

Constitutive Activation of Shh Signaling in Early Postnatal Sox2^{+} GNPs Causes EGL Hyperplasia

We pursued the link between Sox2^{+} GNPs and MB initiation further by testing whether oncogenic transformation specifically targeted to the temporally restricted Sox2^{+} GNP fraction could

(E and F) Representative IF image of tdT reporter expression in the P7 cerebellum (E) and quantification of the percent tdT^{+} cells in the EGL (F) alongside that observed at P2 (gray bars). Bar denotes mean; n = 3 biological replicates from at least two litters for each data point. Scale bar, 100 μm.

(G and H) Representative IF image of tdT reporter expression in the P21 cerebellum (G) and quantification of the percent of tdT^{+} NeuN^{+} cells in the IGL (H) (see Figure S4 for representative images of NeuN IF). Quantification from equivalent EGL regions at P2 are shown as gray bars for comparison. Bar denotes mean; n = 3 biological replicates from at least two litters for each data point. Scale bar, 250 μm.

(I) Strategy for TMX induction in Sox2^{CreER} ; R26^{tdT}; Ptc$^{+/-}$ pups at P1 followed by analysis of reporter expression in PNLs at P21.

(J) Representative IF images of tdT reporter expression in PNLs. N = 2 biological replicates. Scale bars, 100 μm. Cb, cerebellum.

(K) Representative images of Sox2 IF and tdT reporter expression in PNLs. White arrowheads demarcate double-positive cells. Yellow arrowheads demarcate Sox2^{+} cells void of tdT reporter. Scale bars, 20 μm.

(L) Representative images of NeuN IF and tdT reporter expression in PNLs. White arrowheads demarcate clear double-positive cells. Yellow arrowheads demarcate NeuN^{+} cells void of the tdT reporter. Scale bars, 20 μm.

result in MB. To this end, *Sox2*^{CreERT2} mice were crossed to mice harboring a floxed allele of the *Ptc* gene (Uhmann et al., 2007) and/or to mice harboring the *Ptc*^{neo} allele, allowing us to generate four different genotypes for comparison: germline mutants (*Sox2*^{CreERT2} ; *Ptc*$^{+/-}$), single-allele conditional knockouts (KOs) (*Sox2*^{CreERT2} ; *Ptc*$^{L/+}$), double-allele conditional KOs (*Sox2*^{CreERT2} ; *Ptc*$^{L/L}$), and loss of heterozygosity (LOH) conditional KOs (*Sox2*^{CreERT2} ; *Ptc*$^{L/-}$). TMX was delivered at P1, and one cohort was sacrificed at P21 for early-stage analysis, while a second cohort was maintained in a survival assay until the onset of tumor symptoms (Figure 6A).

At P21, *Ptc*$^{+/-}$ germline mutant mice had characteristic focal PNLs, as expected (Figure 6B). Analysis of *Ptc*$^{L/+}$ mice with conditional loss of a single *Ptc* allele revealed small, rare clusters of cells on the surface of the cerebellum (Figure 6C), consistent with early PNLs. Conditional loss of both *Ptc* alleles, however, caused extensive hyperplasia across the entire surface of the cerebellum (Figure 6D), consistent with widespread dysregulation of GNP growth and impaired differentiation. Reduction of the TMX dose from 0.2 mg/pup to 0.05 mg/pup to target a reduced fraction of the Sox2$^+$ population led to focal hyperplasia similar to that seen in germline mutant mice, consistent with a clonal level of initiation (Figure S6A). Last, mice with *Ptc* LOH in the Sox2$^+$ GNP fraction showed aggressive EGL hyperplasia beyond that observed in double *Ptc* KO (Figure 6E). Therefore, constitutively maintained Shh signaling as a consequence of complete *Ptc* loss in the postnatal Sox2$^+$ GNP compartment is sufficient to initiate widespread, aberrant expansion of the EGL, reminiscent of neoplasia.

Rapid MB Formation after Ptc Deletion in Sox2 EGL Cells Mirrors Histopathology of Germline Ptc$^{+/-}$ Model

To test whether the aberrant growth described after SHH activation in Sox2$^+$ cells is reminiscent of hierarchical MB growth, we performed IHC for Sox2, DCX, and NeuN on sections from each of the four genotypes described above at P21. We first analyzed the *Ptc*$^{+/-}$ germline mutants, which revealed a heterogeneous pattern of Sox2, DCX, and NeuN expression (Figure 6F). In the ectopic cell clusters present in the cerebellum of *Ptc*$^{L/+}$ mice, we found clear expression of both DCX and NeuN, but not Sox2 (Figure 6G), suggesting that the conditional loss of a single *Ptc* allele in these circumstances may be insufficient to cause the persistence of Sox2$^+$ progenitors and propagate long-term growth. Analysis of the hyperplastic histology in both the double *Ptc* KO or the LOH mice, however, revealed a pattern strikingly similar to germline *Ptc*$^{+/-}$ mutant histology, with clear and characteristic expression of all markers, including a fraction of relatively rare Sox2$^+$ cells (Figures 6H and 6I).

We next explored whether the hyperplasia caused by conditional *Ptc* loss in the Sox2$^+$ GNP fraction fully progressed to MB. Despite the presence of ectopic cells on the surface of the cerebellum at P21, *Ptc*$^{L/+}$ mice did not develop tumors over 16 weeks of observation (Figure 6J), suggesting a potential requirement for Sox2$^+$ cells in driving long-term growth. Both *Ptc*$^{L/L}$ and *Ptc*$^{L/-}$ mice developed MB, with median survival of 76 and 21 days, respectively (Figure 6J). Control *Ptc*$^{L/L}$ mice given TMX at P7 (after Sox2 expression is almost completely lost from the EGL) did not develop tumors, confirming that the window of vulnerability is limited to a period when Sox2$^+$ cells are present and actively contributing to EGL expansion. Controls not given TMX did not develop tumors, unless they contained the germline *Ptc* mutation, in which case tumors arose with a long latency as expected in this model (Figures S6B and S6C).

Analysis of tissue from *Ptc*$^{L/L}$ tumors showed classic MB histopathology similar to *Ptc*$^{+/-}$ germline mutant tumors (Figures 6K and 6L). IHC revealed a striking similarity in expression of Sox2, DCX, and NeuN between the *Ptc*$^{L/L}$ and *Ptc*$^{+/-}$ models (Figures 6M and 6N), consistent with rare Sox2$^+$ cells maintaining growth of subsequent DCX$^+$ and NeuN$^+$ cell fractions through hierarchical growth. Combined, these data suggest that constitutive Shh pathway activation in the Sox2$^+$ GNP fraction aberrantly perpetuates hierarchical growth and leads to MB. We propose that tumors in the widely used *Ptc* germline mutant mouse model may arise and grow in a similar fashion, with Sox2$^+$ cells defining both the cell of origin and the key cell maintaining growth of these tumors.

Persistence of Sox2 Expression in EGL after Constitutive Shh Activation in Sox2$^+$ GNPs

To test the hypothesis that SHH-subtype MB is caused by the persistence of a Sox2$^+$ GNP, we analyzed the same double *Ptc* KO mouse model at the earliest stages of transformation (Figure 7A).

At P7, gross EGL morphology in KO mice was not notably altered, but an increased number of Sox2$^+$ GNPs in the EGL was observed relative to controls (Figures 7B and 7C). At P14, dramatic focal thickening of the EGL was present in KO mice compared with controls (Figure 7D). We found that the frequency of Sox2$^+$ cells in these lesions was 3.74% ± 0.20%, a frequency consistent with that previously reported in several endpoint SHH-subtype tumor models (Vanner et al., 2014; Figure 7E). In contrast, no Sox2$^+$ cells were seen in the wild-type (WT) P14 EGL. Together, these results indicate that the earliest stages of MB initiation are due to the aberrant persistence of a more primitive Sox2$^+$ GNP cell beyond its appropriate developmental window. We further hypothesize that subsequent progression of MB follows a model of hierarchical growth consistent with normal development, rather than a more simplistic symmetric expansion of a founding mutant stem cell.

DISCUSSION

Multicellular tissue development and homeostasis is characterized by an exquisite balance of cellular proliferation, differentiation, and loss. Dysregulation of the molecular machinery regulating these processes can lead to the aberrant hierarchical growth found to initiate and drive progression of cancer. Here we have demonstrated that expression of the TF Sox2 defines a transient cerebellar precursor cell at the apex of the GN developmental hierarchy in addition to its previously described role as a fourth ventricular NSC. A similar precursor is responsible for maintaining long-term hierarchical growth of SHH-subtype MB following oncogenic transformation (Read et al., 2009; Singh et al., 2004; Vanner et al., 2014; Ward et al., 2009) and strongly supports the hypothesis that SHH-subgroup MB is derived from the dysregulation of this canonical neurogenic process.

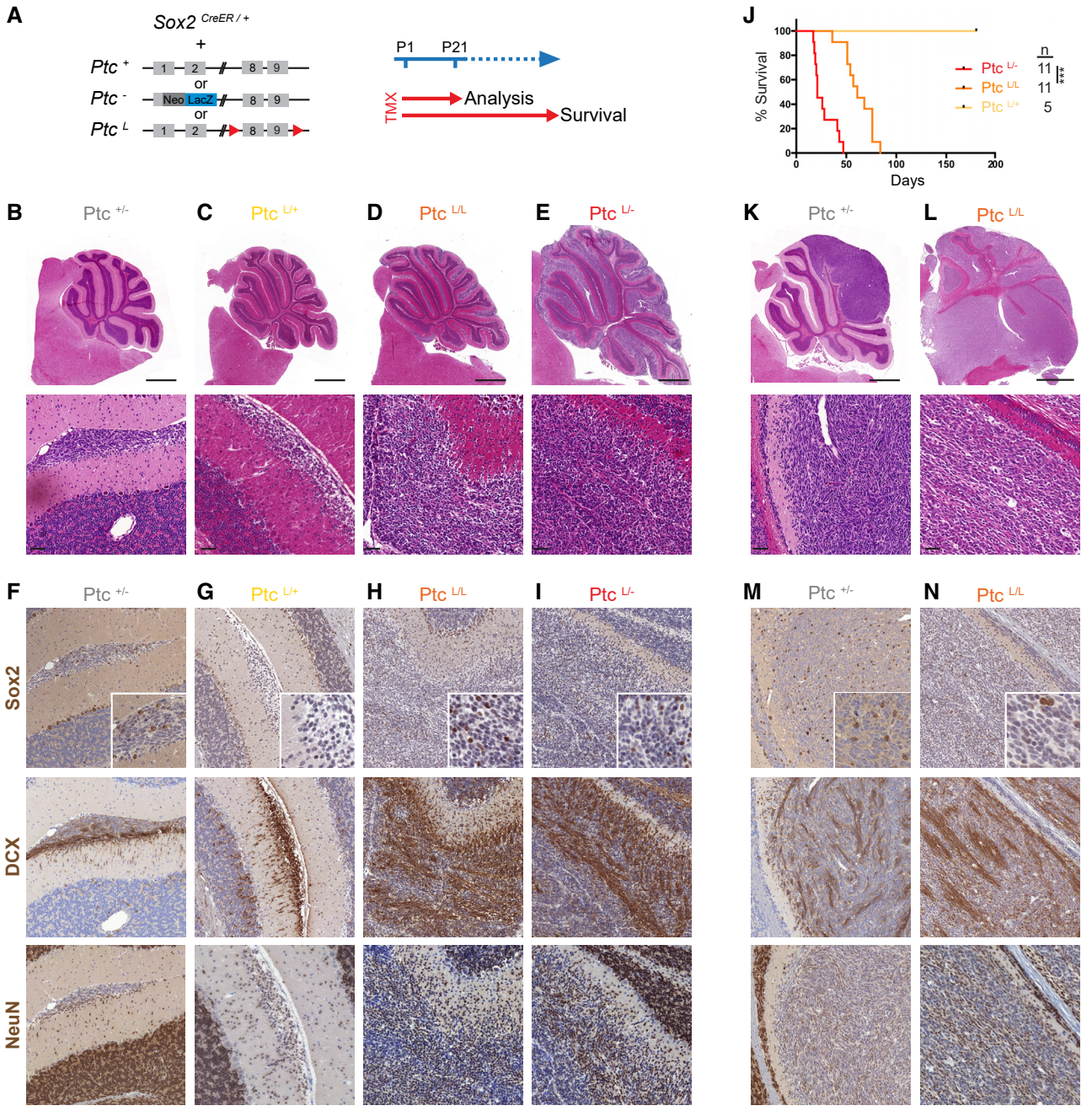

Figure 6. Conditional SHH Activation in Postnatal Sox2^{+} GNPs Causes Rapid Onset of MB Histologically Identical to Ptc Germline Mutant Disease

(A) Mice harboring the Sox2^{CreER} allele were bred to also harbor two of the three depicted *Ptc* alleles and induced with TMX at P1 followed by analysis at P21 or left until endpoint tumor formation.

(B–E) Representative H&E staining of *Ptc*$^{LacZ/+}$ (+/−), *Ptc*$^{LoxP/LacZ}$ (L/−), *Ptc*$^{LoxP/LoxP}$ (L/L), or *Ptc*$^{LoxP/+}$ (L/+) genotypes at P21 showing histology of focal lesions (B and C) and widespread hyperplasia (D and E). Scale bars, 1 mm (top panels) and 50 μm (bottom panels).

(F–I) Representative IHC staining of indicated genotypes at P21 highlighting similar expression of the indicated proteins on consecutive sections. Note lack of Sox2 expression in (G).

(J) Kaplan-Meier survival curves for indicated genotypes after TMX induction at P1. Log rank comparison between L/− and L/L ($p < 0.0001$).

(K and L) Representative H&E staining of endpoint tumors for indicated genotypes. Scale bars, 2 mm (top panels) and 50 μm (bottom panels).

(M and N) Representative IHC staining showing similar expression of key markers in endpoint tumors for indicated genotypes. Insets in top row show magnified view of nuclear Sox2 staining. Images to same scale as (K) and (L).

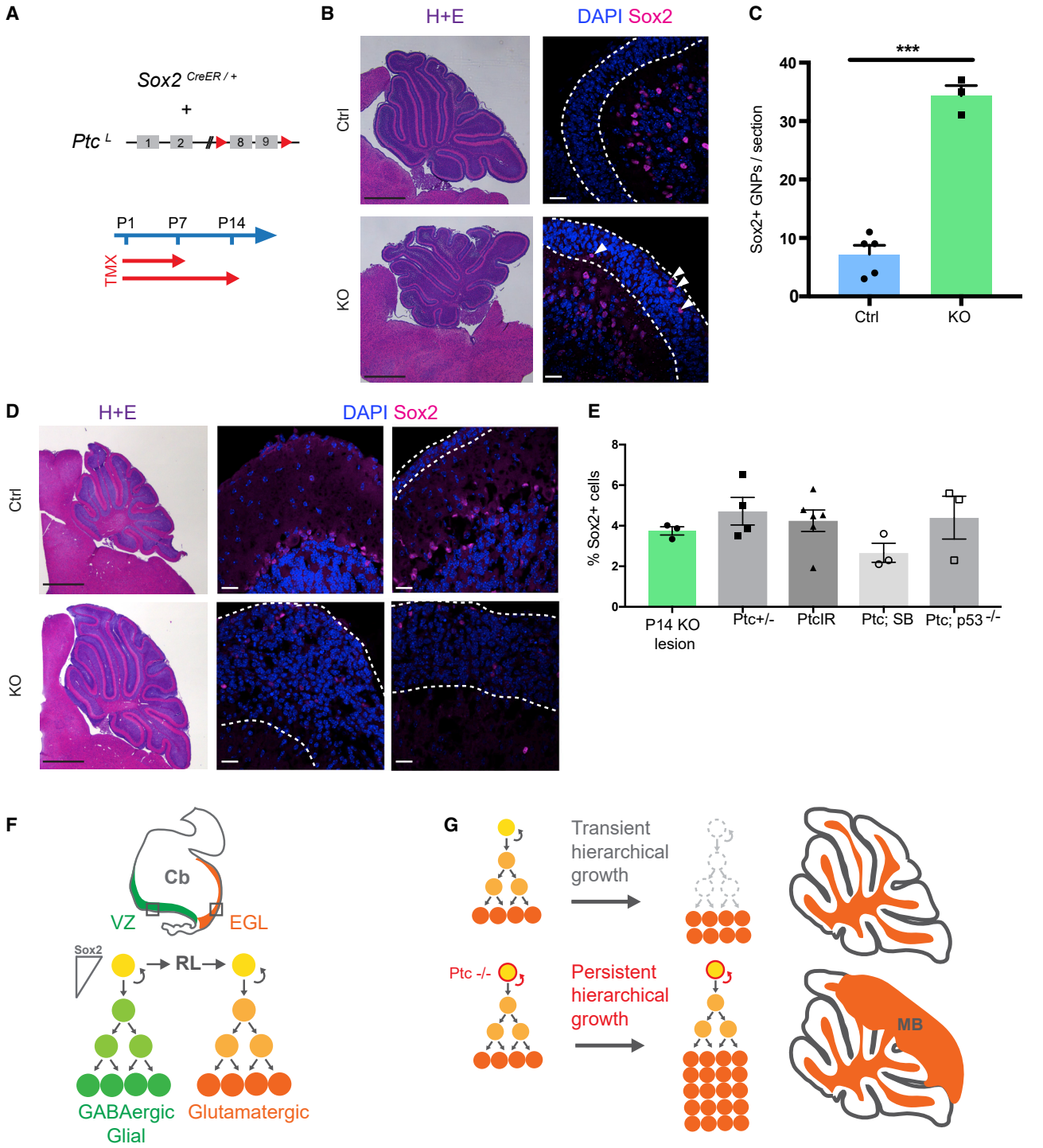

Figure 7. Aberrant Persistence of Sox2$^+$ Cells in the Postnatal EGL at the Root of MB Formation

(A) Mice were bred to harbor two copies of the *Ptc^{LoxP}* allele with or without the Sox2^{creER} allele (top) and chased for the indicated times following TMX administration (bottom).

(B) Representative H$^+$E staining of P7 cerebellum in control (Cre$^-$) and KO (Cre$^+$) mice (left) and representative images of endogenous Sox2 protein (right) detected by IF in the EGL (dotted line). Scale bars, 500 μm (left panels) and 20 μm (right panels). White arrowheads indicate Sox2$^+$ cells.

(C) Quantification of the number of Sox2$^+$ cells per tissue section in the P7 EGL in control and KO mice ($p < 0.001$). Each dot represents a biological replicate. N = 5 in control group, n = 3 in KO group; two-tailed unpaired t test; bars denote mean ± SEM.

(legend continued on next page)

This has implications for the cell of origin, window of vulnerability, mechanism of transformation, and ultimate phenotypic behavior of MB in patients.

Sox2 Expression Defines VZ/RL Progenitors that Give Rise to GNPs

Sox2 is expressed in neurogenic precursors throughout development and is maintained in adult neurogenesis (Ellis et al., 2004). Cell specification in the cerebellum begins with the GABAergic lineage from the VZ, but inductive cues from the adjacent roof plate cells signal the acquisition of glutamatergic cell fate in the RL, defined by expression of the TF *Atoh1* (Machold and Fishell, 2005; Wang et al., 2005). Our identification of Sox2 expression within the RL from E12.5 and the extensive tracing of EGL cells arising from the Sox2$^+$ fraction at E12.5 suggest that the GN lineage is derived from a Sox2$^+$ founder population. The reduction in EGL labeling after lineage tracing from E14.5 is consistent with a critical window of lineage induction at or shortly prior to E12.5.

The cell-specific pattern of Sox2 expression we identified in the RL at E14.5, with Sox2 expressed strongly on the Pax6-low interior aspect and weaker at the Pax6-high exterior aspect is consistent with a molecular compartmentalization of the RL (Schüller et al., 2008) and supports lineage specification occurring closer to the VZ, followed by migration and differentiation within the external aspect and subsequent EGL over a window of 2–3 days. These data are consistent with the view that rather than existing as a morphologically defined region, the RL is better thought of as a zone of dynamic induction at the intercept of molecular signals from the VZ and roof plate (Butts et al., 2014). We propose that transitioning through the inductive territory of the RL changes precursor cell fate but does not affect the role of Sox2 in maintaining a more primitive cell state: a cell that maintains a position at the apex of the hierarchy that drives GN production (Figure 7F).

Persistence of Sox2 Expression in Rare GNPs Suggests a Temporally Regulated Hierarchical Mode of EGL Growth

The EGL is a unique developmental feature of the cerebellum that allows a discrete phase of population-level amplification to multiply a small number of founding GNPs into the most abundant class of neuron in the mammalian brain. We hypothesized that the EGL is composed of functionally heterogeneous cell types, with a more primitive cell type driving the early development of the GN lineage. This is supported by both cell marker staining (*in situ* or through flow cytometry) and scRNA-seq data, with a fraction of Atoh1 lineage-derived cells, marked by Sox2 expression and relative quiescence, displaying characteristics of a more primitive cell state. Consistent with this, the Sox2 lineage trace performed from P1 demonstrates that the Sox2$^+$ cell fraction retains an extensive capacity for contribution to GN development on the basis of the large increase in labeled cells at P7 and P21 compared with the initially labeled fraction at P2. The similar proportions of labeled GNPs at P7 and GNs at P21 are consistent with loss of Sox2 expression prior to this period, marking a shift from self-renewal to differentiation (Legué et al., 2015).

A growing body of evidence has demonstrated the heterogeneous expression of NSC factors in the EGL, such as Nestin (Li et al., 2013; Wojcinski et al., 2017), GFAP (Silbereis et al., 2010), and Olig2 (Schüller et al., 2008), at different developmental time points. We propose that the Sox2$^+$ GNPs we have identified are a functionally and developmentally distinct cell fraction. We analyzed expression of Nestin in addition to *Sox2-eGFP* in perinatal cerebellum but, because of the filamentous nature of the endogenous protein, could not confirm whether all Sox2$^+$ cells are also Nestin$^+$. However, at P4 and under normal conditions, the output of Nestin$^+$ cells in the EGL is interneurons and glia with only minor contributions to the GN lineage, supporting the interpretation that the majority of Nestin$^+$ cells at this time point are of a VZ origin (Li et al., 2013; Wojcinski et al., 2017). Likewise, Wojcinski et al. (2017) described a VZ-derived Nestin$^+$ inner EGL population present at P3 that is capable of undergoing a fate switch to rescue GNP cell numbers in response to widespread injury. In contrast, the Sox2$^+$ cell fraction we identified contributes extensively to the mature GNs under normal conditions, confirming granule lineage identity. We further confirmed this lineage identity through scRNA-seq description of a Sox2^{high} Atoh1^{high} GNP cluster that shows no markers of VZ origin. Last, we performed an Atoh1 lineage trace that revealed the presence of Sox2$^+$ cells in the EGL with both Atoh1 and non-Atoh1 lineage origins, consistent with previous reports that postulate a VZ origin of Nestin$^+$ EGL cells (Li et al., 2013; Wojcinski et al., 2017). Thus, we conclude that Sox2 expression defines two cell types: those VZ-derived progenitors marked by Nestin, Olig2, and GFAP with limited contribution to the GN lineage under normal conditions and a distinct population derived from the RL that function as a source for protracted GN development.

Sox2 Expression Defines Both a Tumor Initiating and Tumor Propagating Cell in the SHH MB Subtype

MB driven by oncogenic activation of the Shh pathway is well established to arise from the GN lineage across various models (Oliver et al., 2005; Schüller et al., 2008), suggesting a similar mode of development in the human disease. Our findings build on this paradigm and support a model in which SHH-subtype MB arises through the aberrant maintenance of a developmental hierarchy through constitutive activation of the Shh pathway in a Sox2$^+$ founding GNP at P1 (Figure 7G). We have demonstrated

(D) Representative H&E staining of P14 cerebellum in control and KO mice (left) and representative images of endogenous Sox2 protein (right) detected by IF in the EGL (dotted line). Scale bars, 500 μm (left panels) and 20 μm (remaining panels).
(E) Quantification of the percentage of Sox2$^+$ cells in representative images of P14 lesions from *Ptc$^{LoxP/LoxP}$* KO mice (green) and comparison with Sox2$^+$ cells previously quantified in *Ptc$^{+/-}$*, PtcIR (*Ptc$^{+/-}$*, 3 Gy radiation on P0), Ptc; SB (*Ptc$^{+/-}$*; T2onc; Sleeping Beauty), and *Ptc; p53$^{-/-}$* endpoint tumors. Dots represent average percentage in individual mice ($p = 0.3066$, one-way ANOVA; mean ± SEM).
(E) Model depicting maintenance of a Sox2$^+$ cell-driven hierarchy from the VZ to the EGL.
(F) Model for MB initiation through the maintenance of a developmental hierarchy.

that the rare postnatal Sox2$^+$ GNP fraction we identified and characterized is readily capable of oncogenic transformation upon Shh activation, resulting in the persistence of key neurogenic programs previously associated with hierarchical MB growth (Vanner et al., 2014). Single-cell analysis of developing cerebellum, in comparison with analysis of human SHH-subtype MBs, continues to support relationships of these tumors to the EGL lineage (Vladoiu et al., 2019).

Our data are consistent with the conclusion that SHH subtype tumors arise in a common cell lineage, but timing of oncogenic lesion as cells transition through the RL and shift from self-renewal to differentiation could dictate outcome and thus account for the differences observed between mouse models. This paradigm is supported by previous reports showing that constitutive SHH activation in stem cells early in cerebellum development (defined by GFAP or Sox2 expression) results in more rapid MB formation and functionally distinct endpoint tumors compared with the same lesion being initiated in a more differentiated Atoh1$^+$ GNP (Ahlfeld et al., 2013; Chow et al., 2014; Schüller et al., 2008; Yang et al., 2008). Temporal differences in susceptibility to tumor initiation have also been noted in postnatal mice, with a reduction in susceptibility to radiation-induced tumorigenesis in *Ptc* mutant mice observed later in the course of EGL expansion (Pazzaglia et al., 2006), notably when Sox2$^+$ GNPs are largely gone. Evidence of spatial heterogeneity in MB formation has also been identified, with tumors arising in a germline *Ptc* mutant model differing in their anatomic location within the rostro-caudal and medio-lateral axes of the cerebellum, correlating with the latency of disease presentation (Ohli et al., 2015). Thus, tumor formation in a particular region is likely associated with its developmental timing (Legué et al., 2015; Machold and Fishell, 2005). Combined, these spatiotemporal differences in MB initiation are consistent with a model of loss of Sox2$^+$ cells in the first few days of postnatal life reducing overall neoplastic potential. However, we do not discount that Sox2$^-$ GNPs also retain the capacity for transformation (indeed, tumors were observed after inducing a SmoM2 driver in Atoh1$^+$ cells at P7, a point after which Sox2 is barely detected in the EGL) (Chow et al., 2014; Ohli et al., 2015). Of note, these tumors could not be propagated *in vitro* under NSC conditions, unlike counterparts induced at earlier stages of development, supporting our hypothesis that the Sox2$^+$ cell compartment remains more favorable for transformation and, importantly, long-term disease propagation.

In the context of SHH pathway activation, we found that the differentiation failure of Sox2$^+$ EGL cells is associated with the later appearance of precursor lesions. Therefore, the initiation of cancer is not necessarily a proliferative event but rather the presence of a persistor with developmental potency that may be the prerequisite. The Sox2$^+$ cells that later drive MB in these models are quiescent (Vanner et al., 2014) and are not shown to be expanded in number over their progeny. The fact that precursor lesions consist of Sox2$^+$, DCX$^+$, and NeuN$^+$ cells suggests that at the earliest neoplastic stages, hierarchies are part and parcel of the establishment of malignancy. As tumors advance, this developmental hierarchy is maintained and contributes to a heterogeneous cellular ecosystem. Understanding these nuanced developmental aberrations will be critical to understanding mechanisms of cancer initiation and establishment.

The presence of dysregulated hierarchical growth is characteristic of many cancer types and implicates the persistence of developmental processes as mechanisms for disease initiation and progression (Lan et al., 2017). Our findings here reinforce the tight link between normal cerebellar development and MB, presenting a clear mechanism for tumor initiation as the aberrant persistence of a progenitor cell state normally lost during development. We therefore propose that Sox2 expression defines both the tumor-initiating cell and the tumor-propagating cell in the SHH subtype of MB.

STAR★METHODS

Detailed methods are provided in the online version of this paper and include the following:

- KEY RESOURCES TABLE
- LEAD CONTACT AND MATERIALS AVAILABILITY
- EXPERIMENTAL MODEL AND SUBJECT DETAILS
  - Ethics statement
  - Mice
- METHOD DETAILS
  - Tamoxifen injections
  - Tissue processing
  - Immunostaining and histology
  - Microscopy
  - Image quantification
  - *In vivo* EdU labeling and detection
  - Fluorescence activated cell sorting
  - Quality control and normalization
  - Clustering analysis and visualization
  - Creation of cell-type specific signatures
  - Cell scoring
  - Pathway analysis and enrichment map
  - Survival analysis
- QUANTIFICATION AND STATISTICAL ANALYSIS
- DATA AND CODE AVAILABILITY

SUPPLEMENTAL INFORMATION

Supplemental Information can be found online at https://doi.org/10.1016/j.celrep.2020.03.075.

ACKNOWLEDGMENTS

We would like to thank the SickKids Imaging Facility, SickKids Laboratory Animal Services, and SickKids-UHN Flow Cytometry Facility for contributions to this work. Research was supported by the Canadian Institutes of Health Research (142434), B.R.A.I.N. Child, and SU2C Canada Cancer Stem Cell Dream Team research funding (SU2C-AACR-DT-19-15) provided by the government of Canada through Genome Canada and with supplemental support from the Ontario Institute for Cancer Research. Stand Up to Cancer Canada is a program of the Entertainment Industry Foundation Canada. Research funding is administered by the American Association for Cancer Research International-Canada, the scientific partner of SU2C Canada. We thank The Hospital for Sick Children Foundation, Jessica's Footprint, and the Hopeful Minds Foundation. P.B.D. holds a Garron Family Chair in Childhood Cancer Research at The Hospital for Sick Children. T.N. and A.K. are supported in part by NIH award U01 MH105989.

AUTHOR CONTRIBUTIONS

Conception: H.J.S., E.L., and P.B.D.; Investigation: H.J.S., E.L., X.L., M.C.V., O.W., C.G., R.J.V., H.W., L.L., and M.K.; Analysis: H.J.S., E.L., K.D., P.D., and P.B.D.; Samples and Reagents: T.N., C.H., and A.K.; Manuscript Preparation: H.J.S., E.L., and P.B.D.; Manuscript Editing and Review: H.J.S., E.L., P.B.D., K.D., X.L., M.C.V., O.W., R.J.V., T.N., and P.D.

DECLARATION OF INTERESTS

The authors declare no competing interests.

Received: June 18, 2019
Revised: August 10, 2019
Accepted: March 23, 2020
Published: April 14, 2020

REFERENCES

Abrahám, H., Tornóczky, T., Kosztolányi, G., and Seress, L. (2001). Cell formation in the cortical layers of the developing human cerebellum. Int. J. Dev. Neurosci. *19*, 53–62.

Ahlfeld, J., Favaro, R., Pagella, P., Kretzschmar, H.A., Nicolis, S., and Schüller, U. (2013). Sox2 requirement in sonic hedgehog-associated medulloblastoma. Cancer Res. *73*, 3796–3807.

Akazawa, C., Ishibashi, M., Shimizu, C., Nakanishi, S., and Kageyama, R. (1995). A mammalian helix-loop-helix factor structurally related to the product of Drosophila proneural gene atonal is a positive transcriptional regulator expressed in the developing nervous system. J. Biol. Chem. *270*, 8730–8738.

Arnold, K., Sarkar, A., Yram, M.A., Polo, J.M., Bronson, R., Sengupta, S., Seandel, M., Geijsen, N., and Hochedlinger, K. (2011). Sox2(+) adult stem and progenitor cells are important for tissue regeneration and survival of mice. Cell Stem Cell *9*, 317–329.

Ashburner, M., Ball, C.A., Blake, J.A., Botstein, D., Butler, H., Cherry, J.M., Davis, A.P., Dolinski, K., Dwight, S.S., Eppig, J.T., et al.; The Gene Ontology Consortium (2000). Gene Ontology: tool for the unification of biology. Nat. Genet. *25*, 25–29.

Ben-Arie, N., McCall, A.E., Berkman, S., Eichele, G., Bellen, H.J., and Zoghbi, H.Y. (1996). Evolutionary conservation of sequence and expression of the bHLH protein Atonal suggests a conserved role in neurogenesis. Hum. Mol. Genet. *5*, 1207–1216.

Ben-Arie, N., Bellen, H.J., Armstrong, D.L., McCall, A.E., Gordadze, P.R., Guo, Q., Matzuk, M.M., and Zoghbi, H.Y. (1997). Math1 is essential for genesis of cerebellar granule neurons. Nature *390*, 169–172.

Butler, A., Hoffman, P., Smibert, P., Papalexi, E., and Satija, R. (2018). Integrating single-cell transcriptomic data across different conditions, technologies, and species. Nat. Biotechnol. *36*, 411–420.

Butts, T., Green, M.J., and Wingate, R.J.T. (2014). Development of the cerebellum: simple steps to make a 'little brain'. Development *141*, 4031–4041.

Chow, K.H., Shin, D.M., Jenkins, M.H., Miller, E.E., Shih, D.J., Choi, S., Low, B.E., Philip, V., Rybinski, B., Bronson, R.T., et al. (2014). Epigenetic states of cells of origin and tumor evolution drive tumor-initiating cell phenotype and tumor heterogeneity. Cancer Res. *74*, 4864–4874.

Cline, M.S., Smoot, M., Cerami, E., Kuchinsky, A., Landys, N., Workman, C., Christmas, R., Avila-Campilo, I., Creech, M., Gross, B., et al. (2007). Integration of biological networks and gene expression data using Cytoscape. Nat. Protoc. *2*, 2366–2382.

Dolecek, T.A., Propp, J.M., Stroup, N.E., and Kruchko, C. (2012). CBTRUS statistical report: primary brain and central nervous system tumors diagnosed in the United States in 2005-2009. Neuro Oncol. *14* (*Suppl 5*), v1–v49.

Ellis, P., Fagan, B.M., Magness, S.T., Hutton, S., Taranova, O., Hayashi, S., McMahon, A., Rao, M., and Pevny, L. (2004). SOX2, a persistent marker for multipotential neural stem cells derived from embryonic stem cells, the embryo or the adult. Dev. Neurosci. *26*, 148–165.

Favaro, R., Valotta, M., Ferri, A.L.M., Latorre, E., Mariani, J., Giachino, C., Lancini, C., Tosetti, V., Ottolenghi, S., Taylor, V., and Nicolis, S.K. (2009). Hippocampal development and neural stem cell maintenance require Sox2-dependent regulation of Shh. Nat. Neurosci. *12*, 1248–1256.

Favaro, R., Appolloni, I., Pellegatta, S., Sanga, A.B., Pagella, P., Gambini, E., Pisati, F., Ottolenghi, S., Foti, M., Finocchiaro, G., et al. (2014). Sox2 is required to maintain cancer stem cells in a mouse model of high-grade oligodendroglioma. Cancer Res. *74*, 1833–1844.

Gangemi, R.M.R., Griffero, F., Marubbi, D., Perera, M., Capra, M.C., Malatesta, P., Ravetti, G.L., Zona, G.L., Daga, A., and Corte, G. (2009). SOX2 silencing in glioblastoma tumor-initiating cells causes stop of proliferation and loss of tumorigenicity. Stem Cells *27*, 40–48.

Goodrich, L.V., Milenković, L., Higgins, K.M., and Scott, M.P. (1997). Altered neural cell fates and medulloblastoma in mouse patched mutants. Science *277*, 1109–1113.

Hatten, M.E. (1999). Central nervous system neuronal migration. Annu. Rev. Neurosci. *22*, 511–539.

Kucera, M., Isserlin, R., Arkhangorodsky, A., and Bader, G.D. (2016). AutoAnnotate: A Cytoscape app for summarizing networks with semantic annotations. F1000Res. *5*, 1717.

Lan, X., Jörg, D.J., Cavalli, F.M.G., Richards, L.M., Nguyen, L.V., Vanner, R.J., Guilhamon, P., Lee, L., Kushida, M.M., Pellacani, D., et al. (2017). Fate mapping of human glioblastoma reveals an invariant stem cell hierarchy. Nature *549*, 227–232.

Legué, E., Riedel, E., and Joyner, A.L. (2015). Clonal analysis reveals granule cell behaviors and compartmentalization that determine the folded morphology of the cerebellum. Development *142*, 1661–1671.

Li, P., Du, F., Yuelling, L.W., Lin, T., Muradimova, R.E., Tricarico, R., Wang, J., Enikolopov, G., Bellacosa, A., Wechsler-Reya, R.J., and Yang, Z.J. (2013). A population of Nestin-expressing progenitors in the cerebellum exhibits increased tumorigenicity. Nat. Neurosci. *16*, 1737–1744.

Lun, A.T.L., Bach, K., and Marioni, J.C. (2016). Pooling across cells to normalize single-cell RNA sequencing data with many zero counts. Genome Biol. *17*, 75.

Machold, R., and Fishell, G. (2005). Math1 is expressed in temporally discrete pools of cerebellar rhombic-lip neural progenitors. Neuron *48*, 17–24.

Madisen, L., Zwingman, T.A., Sunkin, S.M., Oh, S.W., Zariwala, H.A., Gu, H., Ng, L.L., Palmiter, R.D., Hawrylycz, M.J., Jones, A.R., et al. (2010). A robust and high-throughput Cre reporting and characterization system for the whole mouse brain. Nat. Neurosci. *13*, 133–140.

Mansouri, A., Stoykova, A., and Gruss, P. (1994). Pax genes in development. J. Cell Sci. Suppl. *18*, 35–42.

Matei, V., Pauley, S., Kaing, S., Rowitch, D., Beisel, K.W., Morris, K., Feng, F., Jones, K., Lee, J., and Fritzsch, B. (2005). Smaller inner ear sensory epithelia in Neurog 1 null mice are related to earlier hair cell cycle exit. Dev. Dyn. *234*, 633–650.

McInnes, L., Healy, J., and Melville, J. (2018). UMAP: Uniform Manifold Approximation and Projection for Dimension Reduction. arXiv, arXiv:1802.03426. https://arxiv.org/abs/1802.03426.

Merico, D., Isserlin, R., Stueker, O., Emili, A., and Bader, G.D. (2010). Enrichment map: a network-based method for gene-set enrichment visualization and interpretation. PLoS ONE *5*, e13984.

Morris, J.H., Apeltsin, L., Newman, A.M., Baumbach, J., Wittkop, T., Su, G., Bader, G.D., and Ferrin, T.E. (2011). clusterMaker: a multi-algorithm clustering plugin for Cytoscape. BMC Bioinformatics *12*, 436.

Northcott, P.A., Jones, D.T.W., Kool, M., Robinson, G.W., Gilbertson, R.J., Cho, Y.-J., Pomeroy, S.L., Korshunov, A., Lichter, P., Taylor, M.D., and Pfister, S.M. (2012). Medulloblastomics: the end of the beginning. Nat. Rev. Cancer *12*, 818–834.

Oesper, L., Merico, D., Isserlin, R., and Bader, G.D. (2011). WordCloud: a Cytoscape plugin to create a visual semantic summary of networks. Source Code Biol. Med. *6*, 7.

Ohli, J., Neumann, J.E., Grammel, D., and Schüller, U. (2015). Localization of SHH medulloblastoma in mice depends on the age at its initiation. Acta Neuropathol. *130*, 307–309.

Oliver, T.G., Read, T.A., Kessler, J.D., Mehmeti, A., Wells, J.F., Huynh, T.T., Lin, S.M., and Wechsler-Reya, R.J. (2005). Loss of patched and disruption of granule cell development in a pre-neoplastic stage of medulloblastoma. Development *132*, 2425–2439.

Pazzaglia, S., Tanori, M., Mancuso, M., Rebessi, S., Leonardi, S., Di Majo, V., Covelli, V., Atkinson, M.J., Hahn, H., and Saran, A. (2006). Linking DNA damage to medulloblastoma tumorigenesis in patched heterozygous knockout mice. Oncogene *25*, 1165–1173.

Rakic, P., and Sidman, R.L. (1970). Histogenesis of cortical layers in human cerebellum, particularly the lamina dissecans. J. Comp. Neurol. *139*, 473–500.

Read, T.-A., Fogarty, M.P., Markant, S.L., McLendon, R.E., Wei, Z., Ellison, D.W., Febbo, P.G., and Wechsler-Reya, R.J. (2009). Identification of CD15 as a marker for tumor-propagating cells in a mouse model of medulloblastoma. Cancer Cell *15*, 135–147.

Reimand, J., Arak, T., Adler, P., Kolberg, L., Reisberg, S., Peterson, H., and Vilo, J. (2016). g:Profiler-a web server for functional interpretation of gene lists (2016 update). Nucleic Acids Res. *44* (*W1*), W83–W89.

Satija, R., Farrell, J.A., Gennert, D., Schier, A.F., and Regev, A. (2015). Spatial reconstruction of single-cell gene expression data. Nat. Biotechnol. *33*, 495–502.

Schedl, A., Ross, A., Lee, M., Engelkamp, D., Rashbass, P., van Heyningen, V., and Hastie, N.D. (1996). Influence of PAX6 gene dosage on development: overexpression causes severe eye abnormalities. Cell *86*, 71–82.

Schüller, U., Heine, V.M., Mao, J., Kho, A.T., Dillon, A.K., Han, Y.-G., Huillard, E., Sun, T., Ligon, A.H., Qian, Y., et al. (2008). Acquisition of granule neuron precursor identity is a critical determinant of progenitor cell competence to form Shh-induced medulloblastoma. Cancer Cell *14*, 123–134.

Silbereis, J., Heintz, T., Taylor, M.M., Ganat, Y., Ment, L.R., Bordey, A., and Vaccarino, F. (2010). Astroglial cells in the external granular layer are precursors of cerebellar granule neurons in neonates. Mol. Cell. Neurosci. *44*, 362–373.

Singh, S.K., Hawkins, C., Clarke, I.D., Squire, J.A., Bayani, J., Hide, T., Henkelman, R.M., Cusimano, M.D., and Dirks, P.B. (2004). Identification of human brain tumour initiating cells. Nature *432*, 396–401.

Sudarov, A., Turnbull, R.K., Kim, E.J., Lebel-Potter, M., Guillemot, F., and Joyner, A.L. (2011). Ascl1 genetics reveals insights into cerebellum local circuit assembly. J. Neurosci. *31*, 11055–11069.

Tamayo-Orrego, L., Wu, C.-L., Bouchard, N., Khedher, A., Swikert, S.M., Remke, M., Skowron, P., Taylor, M.D., and Charron, F. (2016). Evasion of cell senescence leads to medulloblastoma progression. Cell Rep. *14*, 2925–2937.

The Gene Ontology Consortium (2019). The Gene Ontology Resource: 20 years and still GOing strong. Nucleic Acids Res. *47* (*D1*), D330–D338.

Tirosh, I., Venteicher, A.S., Hebert, C., Escalante, L.E., Patel, A.P., Yizhak, K., Fisher, J.M., Rodman, C., Mount, C., Filbin, M.G., et al. (2016). Single-cell RNA-seq supports a developmental hierarchy in human oligodendroglioma. Nature *539*, 309–313.

Uhmann, A., Dittmann, K., Nitzki, F., Dressel, R., Koleva, M., Frommhold, A., Zibat, A., Binder, C., Adham, I., Nitsche, M., et al. (2007). The Hedgehog receptor Patched controls lymphoid lineage commitment. Blood *110*, 1814–1823.

Vanner, R.J., Remke, M., Gallo, M., Selvadurai, H.J., Coutinho, F., Lee, L., Kushida, M., Head, R., Morrissy, S., Zhu, X., et al. (2014). Quiescent sox2(+) cells drive hierarchical growth and relapse in sonic hedgehog subgroup medulloblastoma. Cancer Cell *26*, 33–47.

Vladoiu, M.C., El-Hamamy, I., Donovan, L.K., Farooq, H., Holgado, B.L., Sundaravadanam, Y., Ramaswamy, V., Hendrikse, L.D., Kumar, S., Mack, S.C., et al. (2019). Childhood cerebellar tumours mirror conserved fetal transcriptional programs. Nature *572*, 67–73.

Wallace, V.A. (1999). Purkinje-cell-derived Sonic hedgehog regulates granule neuron precursor cell proliferation in the developing mouse cerebellum. Curr. Biol. *9*, 445–448.

Wang, V.Y., Rose, M.F., and Zoghbi, H.Y. (2005). Math1 expression redefines the rhombic lip derivatives and reveals novel lineages within the brainstem and cerebellum. Neuron *48*, 31–43.

Ward, R.J., Lee, L., Graham, K., Satkunendran, T., Yoshikawa, K., Ling, E., Harper, L., Austin, R., Nieuwenhuis, E., Clarke, I.D., et al. (2009). Multipotent CD15+ cancer stem cells in patched-1-deficient mouse medulloblastoma. Cancer Res. *69*, 4682–4690.

Wechsler-Reya, R.J., and Scott, M.P. (1999). Control of neuronal precursor proliferation in the cerebellum by Sonic Hedgehog. Neuron *22*, 103–114.

Wingate, R.J. (2001). The rhombic lip and early cerebellar development. Curr. Opin. Neurobiol. *11*, 82–88.

Wojcinski, A., Lawton, A.K., Bayin, N.S., Lao, Z., Stephen, D.N., and Joyner, A.L. (2017). Cerebellar granule cell replenishment postinjury by adaptive reprogramming of Nestin^{+} progenitors. Nat. Neurosci. *20*, 1361–1370.

Wojcinski, A., Morabito, M., Lawton, A.K., Stephen, D.N., and Joyner, A.L. (2019). Genetic deletion of genes in the cerebellar rhombic lip lineage can stimulate compensation through adaptive reprogramming of ventricular zone-derived progenitors. Neural Dev. *14*, 4.

Yang, Z.-J., Ellis, T., Markant, S.L., Read, T.-A., Kessler, J.D., Bourboulas, M., Schüller, U., Machold, R., Fishell, G., Rowitch, D.H., et al. (2008). Medulloblastoma can be initiated by deletion of Patched in lineage-restricted progenitors or stem cells. Cancer Cell *14*, 135–145.

Yeung, J., Ha, T.J., Swanson, D.J., Choi, K., Tong, Y., and Goldowitz, D. (2014). Wls provides a new compartmental view of the rhombic lip in mouse cerebellar development. J. Neurosci. *34*, 12527–12537.

STAR★METHODS

KEY RESOURCES TABLE

REAGENT or RESOURCE	SOURCE	IDENTIFIER
Antibodies		
Rabbit anti-Sox2	Abcam	Cat# ab97959; RRID:AB_2341193
Mouse anti-Sox2	Abcam	Cat# ab79351; RRID:AB_10710406
Goat anti-Sox2	R&D Systems	Cat# AF2018; RRID:AB_355110
Rabbit anti-DCX	Abcam	Cat# ab18723; RRID:AB_732011
Mouse anti-NeuN	EMD Millipore	Cat# MAB377; RRID:AB_2298767
Rabbit anti-Olig2	EMD Millipore	Cat# AB9610; RRID:AB_570666
Rabbit anti-Pax6	Biolegend	Cat# 901301; RRID:AB_2565003
Mouse anti-Nestin	BD Biosciences	Cat# 556309; RRID:AB_396354
Biological Samples		
Human fetal brain tissue	This paper	N/A
Chemicals, Peptides, and Recombinant Proteins		
Tamoxifen	Sigma	Cat# T5648
Bloxall	Vector Laboratories	Cat# SP-6000, RRID:AB_2336257
5-Ethynyl-20-deoxyuridine (EdU)	Invitrogen	Cat# A10044
Critical Commercial Assays		
DAB Substrate Kit (3,3′-diaminobenzidine)	Vector Laboratories	Cat# SK-4100, RRID:AB_2336382
Vector M.O.M. ImmPRESS Kit	Vector Laboratories	Cat# MP-2400, RRID:AB_2336832
ImmPRESS Anti-Rabbit Ig Reagent antibody	Vector Laboratories	Cat# MP-7401, RRID:AB_2336529
Click-iT Plus EdU Alexa Fluor 647 Imaging Kit	ThermoFisher	Cat# C10640
Deposited Data		
Filtered scRNaseq gene matrix from the P0 and P7 murine hindbrain	Vladoiu et al., 2019	GEO: GSE118068
Experimental Models: Organisms/Strains		
Sox2^{eGFP} (Sox2^{tm1Lpev})	Provided by Dr. Freda Miller; Ellis et al., 2004	N/A
Sox2^{CreER} (B6;129S-*Sox2$^{tm1(cre/ERT2)Hoch}$*/J)	Provided by Dr. Konrad Hochedlinger; Arnold et al., 2011	JAX: 017593
R26^{tdT} (B6;129S6-*Gt(ROSA)26Sor$^{tm14(CAG-tdTomato)Hze}$*/J)	The Jackson Laboratory; Madisen et al., 2010	JAX: 007914
Ptc1^{LacZ} (Ptch1^{tm1Mps}/J)	The Jackson Laboratory; Goodrich et al., 1997	JAX: 003081
Ptc1^{LoxP} (B6N.129-Ptch1^{tm1Hahn}/J)	The Jackson Laboratory; Uhmann et al., 2007	JAX: 012457
Atoh1^{cre} (B6.Cg-Tg(Atoh1-cre)1Bfri/J)	Provided by Dr. Norman Rosenblum; Matei et al., 2005	JAX: 011104
WT CD1 (Crl:CD1(ICR))	Charles River Laboratories	CRL: 022
Software and Algorithms		
ImageJ	ImageJ	RRID:SCR_003070
Prism 7 and Prism 8	GraphPad	RRID:SCR_002798
Adobe Photoshop CS5	Adobe Systems	RRID:SCR_014199
NIS-Elements Image Acquisition Software	Nikon	RRID:SCR_014329
Seurat v3.0	Satija Lab	RRID:SCR_016341
Enrichment Map v3.1.0	Merico et al., 2010	RRID:SCR_016052
Volocity Image Acquisition Software	Perkin Elmer	RRID:SCR_002668

(*Continued on next page*)

Continued

REAGENT or RESOURCE	SOURCE	IDENTIFIER
Pannoramic Viewer Software	3Dhistech	RRID:SCR_017654
FlowJo v10	BD Biosciences	RRID:SCR_008520
Scran 1.10.2	Lun et al., 2016	RRID:SCR_016944
UMAP 0.2.0.0	McInnes et al., 2018	https://github.com/lmcinnes/umap
gProfileR v0.6.7	Reimand et al., 2016	RRID:SCR_006809
Cytoscape v3.7.0	Cline et al., 2007	RRID:SCR_003032
Autoannotate v1.3	Kucera et al., 2016	https://baderlab.org/Software/AutoAnnotate
Word Cloud v3.1.1	Oesper et al., 2011	http://baderlab.org/Software/WordCloudPlugin/UserManual
clusterMaker2 v1.2.1	Morris et al., 2011	http://apps.cytoscape.org/apps/clustermaker2
Gene Ontology Biological Pathways Database	Ashburner et al., 2000; The Gene Ontology Consortium, 2019	RRID:SCR_002811

LEAD CONTACT AND MATERIALS AVAILABILITY

Further information and requests for resources and reagents should be made to the Lead Contact, Dr. Peter Dirks (peter.dirks@sickkids.ca).

This study did not generate new unique reagents.

EXPERIMENTAL MODEL AND SUBJECT DETAILS

Ethics statement

All experiments carried out on mice were approved by the Hospital for Sick Children's Animal Care Committee (protocols 1000035382, 1000039831, and 1000046813) in accordance with the Canadian Council on Animal Care Guidelines. De-identified, archival primary human tissue was obtained with consent in strict observance of the legal and institutional ethical regulations. Protocols were approved by the Human Gamete, Embryo, and Stem Cell Research Committee at the University of California, San Francisco, and the Research Ethics Board at the Hospital for Sick Children, Toronto.

Mice

Mice had free access to rodent chow and water in a 12 hour dark-light cycle room. All mice were healthy with no apparent behavioral phenotypes. For all mouse studies, mice of either sex were used. Ages of all mice used in experiments are indicated in the figure legends. The following transgenic mouse strains were purchased from the Jackson Laboratory: *Ptc1*^{LacZ} *(Ptch1*^{tm1Mps}*/J)* (JAX stock #003081) (Goodrich et al., 1997), *Ptc1*^{LoxP} (B6N.129-Ptch1^{tm1Hahn}/J) (JAX stock #012457) (Uhmann et al., 2007), *R26*^{tdT} (B6;129S6-*Gt(ROSA)26Sor*$^{tm14(CAG-tdTomato)Hze}$/J) (JAX stock #007914) (Madisen et al., 2010). *Sox2*^{eGFP} (Sox2^{tm1Lpev}) mice (Ellis et al., 2004) were provided by Dr. Freda Miller, Toronto, Hospital for Sick Children. *Sox2*^{CreER} (B6;129S-*Sox2*$^{tm1(cre/ERT2)Hoch}$/J) mice (Arnold et al., 2011) (JAX stock #017593) were provided by Dr. Konrad Hochedlinger, Boston, Massachussetts General Hospital. Atoh1^{cre} (B6.Cg-Tg(Atoh1-cre)1Bfri/J) mice (Matei et al., 2005) (JAX stock #011104) were provided by Dr. Norman Rosenblum, Toronto, Hospital for Sick Children. CD1 mice were purchased from Charles River Laboratories (strain code: 022). All mice were bred and genotyped as recommended by the Jackson Laboratory, except *Sox2*^{eGFP} (Sox2^{tm1Lpev}) mice which were genotyped based on Ellis et al., 2004.

METHOD DETAILS

Tamoxifen injections

All mouse lines were maintained on a mixed genetic background and genotyped according to original references. The day a vaginal plug was observed was taken as E0.5 and day of birth was taken as P0. Cre activity was induced in embryonic mice by delivery of a single dose of 150 mg / Kg TMX dissolved in 10% EtOH / sesame oil on the specified day by oral gavage. Cre activity was induced in new born pups by delivery of a single dose of 0.2 mg TMX prepared as above by subcutaneous injection. This was reduced to 0.05 mg per pup to examine focal lesion generation. Mice aged P7 and up were treated with 150 mg/Kg TMX prepared as above by subcutaneous injection. Sox2^{WT} ; R26^{tdT} littermates were used as negative controls for each experiment, along with Sox2^{CreER} ; R26^{tdT} cohorts without TMX administration.

Tissue processing

Tissue from postnatal mice was dissected after transcardial perfusion of cold PBS followed by 4% PFA and subsequently fixed overnight at 4°C immersed in 4% PFA. Tissue from embryos was dissected and fixed overnight as above. For immunofluorescence (IF), tissue was washed and cryoprotected in 30% sucrose / PBS for 24-48 hours prior to snap freezing in either a 1:1 solution of 30% sucrose and OCT embedding media or 100% OCT. Frozen sections were cut sagittally at a thickness of 16 μm on a cryostat and kept at −20°C until staining. For experiments assessing the persistence of $Sox2^{+}$ cells in the developing EGL, sections were cut at a thickness of 25 μm. For immunohistochemistry (IHC) and histological staining tissue was washed, dehydrated in EtOH, wax embedded and cut sagittally at thickness of 10 μm on a microtome. Resected primary human material was fixed overnight in formalin and processed for frozen or wax sectioning as above.

Immunostaining and histology

Standard protocols were followed. For IF, frozen sections were thawed, washed in PBS and blocked in a solution of 10% normal goat serum / 0.1% Triton-X / PBS. Primary antibodies were incubated overnight at 4°C at the specified concentrations in blocking solution. Goat anti-rabbit/mouse 488/568/647 fluorophore-conjugated secondary antibodies (Molecular Probes) were used at a concentration of 1:200 in blocking solution alongside DAPI or TOPRO at a concentration of 1:1000 for one hour at room temperature. Slides were mounted in Fluorescence Mounting Media (DAKO) and air-dried in the dark overnight before imaging. For IHC, FFPE sections were de-waxed in xylene and rehydrated in graded EtOH solutions before washing in PBS and blocking endogenous peroxidase activity with Bloxall (Vector Laboratories). Antigen retrieval was performed by boiling in Citrate buffer (pH 6.0) in a microwave under pressure for five minutes. Blocking, primary antibody incubation and secondary steps were performed following the ImmPRESS RP Anti-Rabbit IgG (Peroxidase) Polymer Detection Kit (Vector Laboratories). For primary antibodies raised in mouse, a Mouse on Mouse (M.O.M.) ImmPRESS HRP (Peroxidase) Polymer kit (Vector Laboratories) was used. Staining was visualized with a DAB Peroxidase (HRP) Substrate Kit (Vector Laboratories) and sections were counterstained with Mayer's Hematoxylin (Sigma). For each experiment sections were also stained with all but the primary antibody to control for background staining levels. Hematoxylin and Eosin staining for histology was performed using standard methods. In all cases analyses were performed on at least three biological replicates.

For immunofluorescence, the following antibodies were used: Rb anti-Sox2 (1:500, Abcam, ab97959), Ms anti-Sox2 (1:100, Abcam, ab79351), Gt anti-Sox2 (1:200, R&D Systems, AF2018), Rb anti-DCX (1:500, Abcam, ab18723), Ms anti-NeuN (1:500, EMD Millipore, MAB377), Rb anti-Olig2 (1:500, EMD Millipore, AB9610), Rb anti-Pax6 (1:300, Biolegend, 901301), Ms anti-Nestin (1:500, BD Biosciences, 556309). For immunohistochemistry, the following antibodies were used: Rb anti-Sox2 (1:500, Abcam, ab97959), Ms anti-Sox2 (1:1000, Abcam, ab79351), Rb anti-DCX (1:5000, Abcam, ab18723), and Ms anti-NeuN (1:1000, EMD Millipore, MAB377).

Microscopy

IHC images were acquired on a 3Dhistech Pannoramic 250 Flash II Slide Scanner and processed in 3Dhistech Pannoramic Viewer software. $H^{+}E$ images were acquired on a Nikon Eclipse Ci light microscope with a Nikon DS-Fi2. Wide field fluorescent images were acquired on a Leica DMI6000B light microscope with a Leica DM. Confocal microscopy was performed on either a) a Quorum spinning disc confocal system consisting of a Olympus IX81 inverted fluorescence microscope equipped with a Hamamatsu C9100-13 back-thinned EM-CCD camera and acquired using Volocity acquisition software (Perkin Elmer); or b) a Nikon A1R Si Point Scanning Confocal system consisting of a Nikon Eclipse Ti microscope and 4 PMT, 1 32-channel spectral PMT detector and acquired using NIS-Elements, Picoquant SymPhoTime 64 acquisition software. All images were analyzed in raw format and prepared in an unbiased manner for publication in Photoshop CS5 (Adobe).

Image quantification

For quantification of the tdT lineage trace presented in Figure 5 we imaged each lobule from a representative vermis and hemisphere section from three mice and quantified only the medial section. For P2 and P7 stages, we imaged the crown of each. Total $DAPI^{+}$ cells present in the EGL (defined morphologically) were counted alongside $DAPI^{+}/tdT^{+}$ cells. For the P21 time point we also performed IF for NeuN in order to differentiate between tdT^{+} GNs and any other lineage that may be traced (e.g., astrocytes) and imaged the IGL at the crown of each lobule. Total $NeuN^{+}$ cells and $NeuN^{+}/tdT^{+}$ cells were quantified. Quantification in all cases was performed on channels independently with the raw images in ImageJ.

In vivo EdU labeling and detection

Wild-type CD1 mice were administered 100 μg of EdU (Invitrogen) intraperitoneally on P0. EdU was dissolved in 0.9% saline solution. Animals were sacrificed 3 hours later and tissue was collected and processed for immunofluorescent staining as previously described. EdU incorporation was later detected using the Click-iT Plus EdU Alexa Fluor 647 Imaging Kit (ThermoFisher) according to the manufacturer's protocol. Samples were imaged and quantified as previously described.

Fluorescence activated cell sorting

The brains of P0 $Atoh1^{cre}/tdT/Sox2^{eGFP}$ mice were dissected and stored on a Petri dish on ice. Brains were then genotyped visually for GFP or tdT expression using a Leica DMI6000B light microscope. The hindbrain, including the brain stem, was dissociated mechanically in 0.1% BSA/PBS supplemented with DNase I. Cells were passed through a 35 μM nylon filter and stained

with DAPI before live-cell sorting using a Beckman Coulter MoFlo Astrios. Data were analyzed and quantified using FlowJo (v10) software.

Quality control and normalization

The filtered scRNaseq gene matrix of the P0 and P7 mouse hindbrain was downloaded (Vladoiu et al., 2019) and generated using the 10x Genomics platform. Data was processed for quality control and normalized as described previously (Vladoiu et al., 2019) by adapting the Seurat (Satija et al., 2015) and Scran (Lun et al., 2016) pipelines.

Clustering analysis and visualization

Analysis was done as previously described unless otherwise specified (Vladoiu et al., 2019). Briefly, highly variable genes excluding cell cycle related (Tirosh et al., 2016) were selected in order to perform principal component analysis, followed by k-nearest neighbors clustering using Seurat's standard pipeline (Butler et al., 2018; Satija et al., 2015). The number of clusters was selected by examining the uniqueness of the top marker genes of each individual cluster. We visualized clusters using both *t*-distributed stochastic neighbor embedding (*t*-SNE) and Uniform Manifold Approximation and Projection for Dimension Reduction (UMAP) (McInnes et al., 2018).

Creation of cell-type specific signatures

Differential gene expression was calculated using Seurat's likelihood ratio test method. We filtered genes expressed in less than 10% of cells and used a log fold-change threshold of 0.25. The resulting gene sets were used to build a signature for each cell type. To generate the Atoh1^{high} Sox2^{high} P0 GNP signature, the top 200 differentially expressed genes were selected (filtered by p value).

Cell scoring

For cells that were scored for enrichment of a given signature, the reference signature was first filtered to remove any genes not detected in the scRNaseq experiment. Enrichment of the signature in individual cells was then calculated by normalizing the average expression of all genes in the signature to the average expression of all genes detected in the scRNaseq experiment. For the Shh score, Gene Ontology pathway GO:0007224 was used and genes were obtained from the Bader lab gene set (Mouse_GOBP_AllPathways_no_GO_iea_April_01_2019_symbol.gmt).

Pathway analysis and enrichment map

The threshold for genes tested was set to those expressed in at least 1% of cells as the cluster of interest (cluster 3) accounted for < 5% of total cells. Instead of log fold-change, differentially expressed genes were filtered by a Bonferonni corrected p value of < 5%. Differentially expressed genes were then subjected to a pathway analysis using the Gene Ontology (GO) Biological Pathways database (Ashburner et al., 2000; The Gene Ontology Consortium, 2019). Pathway analysis was performed with g:Profiler using the gProfileR package (Reimand et al., 2016). A custom background was used which comprised all genes detected by the 10x platform. GO terms were filtered for a minimum gene set size of 5 and maximum gene set size of 2000. Any annotations that were 'inferred from electronic annotation' were excluded (exclude.iea = TRUE). P value correction was done using the g:SCS method and pathways were filtered at an adjusted P value threshold of 0.10. The enrichment map was generated via Cytoscape (Cline et al., 2007) using the following applications: Enrichment Map (Merico et al., 2010), AutoAnnotate (Kucera et al., 2016), clusterMaker2 (Morris et al., 2011), and WordCloud (Oesper et al., 2011).

Survival analysis

Mice in the *Ptc* knock out or loss of heterozygosity experiment presented in Figure 6 were monitored daily following TMX injection at P1 or P7 and sacrificed at the first onset of neurological symptoms. Log-rank (Mantel-Cox) survival analyses were performed in Prism 7 (GraphPad).

QUANTIFICATION AND STATISTICAL ANALYSIS

Statistical analyses were performed in GraphPad Prism 7. For data displayed as violin plots, graphs and corresponding statistical analyses were performed in GraphPad Prism 8. Unless otherwise stated, in all figures * = $p < 0.05$; ** = $p < 0.01$; *** = $p < 0.001$; **** = $p < 0.0001$. Details of specific tests and sample numbers are reported in figure legends.

DATA AND CODE AVAILABILITY

The following packages were used for data analysis: Seurat v3.0, gProfileR v0.6.7, Cytoscape v3.7.0, Enrichment Map v3.1.0, AutoAnnotate v1.3, clusterMaker2 v1.2.1, and WordCloud v3.1.1.